INTERNATIONAL ATOMIC ENERGY AGENCY
UNITED NATIONS EDUCATIONAL, SCIENTIFIC AND CULTURAL ORGANIZATION
INTERNATIONAL CENTRE FOR THEORETICAL PHYSICS
I.C.T.P., P.O. BOX 586, 34100 TRIESTE, ITALY. CABLE CENTRATOM TRIESTE

H4.SMR/453-11

TRAINING COLLEGE ON PHYSICS AND CHARACTERIZATION OF LASERS AND OPTICAL FIBRES

(5 February - 2 March 1990)

SOLID STATE AND SEMICONDUCTOR LASERS PHYSICS AND DEVICES

A. Mooradian

LECTURE NOTES
FOR

PHYSICS & CHARACTERIZATION OF LASERS AND
OPTICAL FIBERS
INTERNATIONAL CENTRE FOR THEORETICAL PHYSICS
TRIESTE, ITALY
FEBRUARY, 1990

SOLID STATE AND SEMICONDUCTOR LASERS
PHYSICS AND DEVICES

A. MOORADIAN
MIT LINCOLN LABORATORY
USA

SPECTRAL CHARACTERISTICS OF SEMICONDUCTOR DIODE LASERS

A. Mooradian

Lincoln Laboratory, Massachusetts Institute of Technology
Lexington, Massachusetts 02173-0073

INTRODUCTION

The spectral linewidth and phase noise characteristics of single-frequency semiconductor diode lasers have become quite important for application to such areas as frequency standards, fiber optical sensors, laser gyros, and optical communications. This work describes the spectral broadening mechanisms which have been observed for monolithic (GaAl)As and lead-salt diode lasers as well as the spectral characteristics of external-cavity controlled (GaAl)As diode lasers.

LINEWIDTH BROADENING MECHANISMS

Power Dependent Broadening

Many of the fundamental broadening mechanisms for a semiconductor laser can be conveniently described with the help of Fig. 1. The laser field amplitude is represented in the complex plane by

$$E = CI^{1/2} \exp(i\phi) \quad , \qquad (1)$$

where I and ϕ are the time dependent intensity and phase of the laser field, and C is a dimensional constant. When a spontaneous emission photon is radiated into the mode of the laser field, it adds as a small vector with a random phase θ_i to produce a new field intensity $I + \Delta I$ with a phase change of $\Delta\phi$. Because these spontaneous emission events are random, the phase ϕ executes Brownian motion and has a Gaussian probability distribution. Lax[1] has performed a very extensive analysis of noise in laser oscillators and has shown that the

autocorrelation function of a laser field can be written approximately as

$$\langle E(t)^*E(0)\rangle = E(0)^2 \exp(-\langle\Delta\phi^2\rangle/2)\exp(i\omega t) \qquad (2)$$

where

$$\Delta\phi = \phi(t)-\phi(0) \qquad (3)$$

and ω is the laser angular frequency. Equation (2) has neglected amplitude flucuations. The power spectrum is then obtained by taking the Fourier transform of the autocorrelation function. The laser linewidth originally described by the Schawlow-Townes theory[2] in which only the quantum phase fluctuations were considered produced an expression for the linewidth given by

$$2\Gamma = (\pi h\nu\Gamma_c^2/P_c)n_{sp} \quad , \qquad (4)$$

where 2Γ is the full width at half-maximum of the laser line at frequency ν, P_c is the intracavity power emitted by the stimulated emission, and Γ_c is the passive resonator linewidth given by

$$\Gamma_c = c(\beta L-\ell nR)/2\pi nL \quad , \qquad (5)$$

where n is an effective refractive index including dispersion, β is the mode loss coefficient, L is the cavity length, n_{sp} is a population factor described below, and R is the facet reflectivity. Equation (4) applies to the case where the driving noise source, spontaneous emission, is homogeneous and band limited. The factor n_{sp} in Eq. (4) is the ratio of spontaneous emission rate per mode to the stimulated emission rate per laser photon and for a semiconductor laser is given by

$$n_{sp} = \frac{f_c(E_2)[1-f_v(E_1)]}{f_c(E_2)-f_v(E_1)} \quad , \qquad (6)$$

where $f_c(E_2)$ and $f_v(E_1)$ are the occupancy factors for the upper and lower laser levels, respectively. Equation (6) becomes for Fermi or Maxwellian statistics

$$n_{sp} = \{1-\exp[(h\nu+E_{FV}-E_{FC})/kT]\}^{-1} \quad , \qquad (7)$$

where E_{FC} and E_{FV} are the conduction-band and valence-band quasi-Fermi levels, k is Bolzmann's constant, and T is the temperature. In most lasers n_{sp} is nearly unity because for four-level devices the terminal state is usually empty. For semiconductor lasers with non-degenerate carrier distribution functions n_{sp} is greater than unity at room temperature. For (GaAl)As diode lasers, $(h\nu+E_{FV}-E_{FC}) \approx$ 15 meV at room temperature[3] and n_{sp} is about 2.3, approaching unity at 77 K. This spontaneous emission factor can be physically

understood by noting that a finite terminal state population can cause absorption of laser photons which in turn will produce more spontaneous photons to be radiated into the laser mode with random phase.

The Schawlow-Townes description of laser linewidth has been shown to be inadequate to describe the results of measurements for (GaAl)As diode lasers.[4] An additional broadening mechanism which was considered but neglected as sizable effect by Lax[1,5] and Haug and Haken[6] has been reexamined recently by Henry,[7] and later by Vahala and Yariv.[8] This additional broadening mechanism can be understood by again referring to Fig. 1. In addition to the usual broadening caused by phase fluctuations arising from spontaneous emission events, there is an additional contribution to the line broadening which comes from a phase change associated with the laser field intensity change induced by spontaneous emission. The carrier density and hence gain will fluctuate to restore the laser field amplitude to the steady-state value. The change in the gain or imaginary part of the refractive index arising from this carrier density change is accompanied by a change in the real part of the refractive index. The time it takes to restore equilibrium is the relaxation time of about one nanosecond, and this is long enough for an observable broadening of the laser linewidth to occur. This additional broadening mechanism modifies the original Schawlow-Townes linewidth to give[7,8]

$$2\Gamma = (\pi h\nu\Gamma_c^2/P_c)n_{sp}\,(1+\alpha^2) \quad , \qquad (8)$$

where α is the ratio of change in the real part of refractive index to the change in the imaginary part of refractive index due to spontaneous emission events over the same period of time. The real part of refractive index change can be related to laser mode shifts with change in carrier density using

$$\Delta n_r = (n/\lambda)\Delta\lambda \quad , \qquad (9)$$

while the imaginary part of the refractive index change can be related to gain changes as a function of carrier density using

$$\Delta n_i = -(c/2\omega)\Delta g \quad . \qquad (10)$$

All of the above contributions to laser linewidth can be seen to be inversely dependent upon laser power from Fig. 1 since the amplitude of the spontaneous emission photons remains fixed as the laser intensity grows. This additional line broadening mechanism is similar to the problem of a detuned gas laser treated by Lax[1,5] where the cavity resonance and the optical transition frequencies do not coincide. Haug and Haken[6] also discussed a $1+\alpha^2$ contribution to the laser linewidth but like Lax did not consider it as significant.

The linewidth problem has been discussed in various ways including the Van der Pol oscillator model[1,9,10] in which the frequency

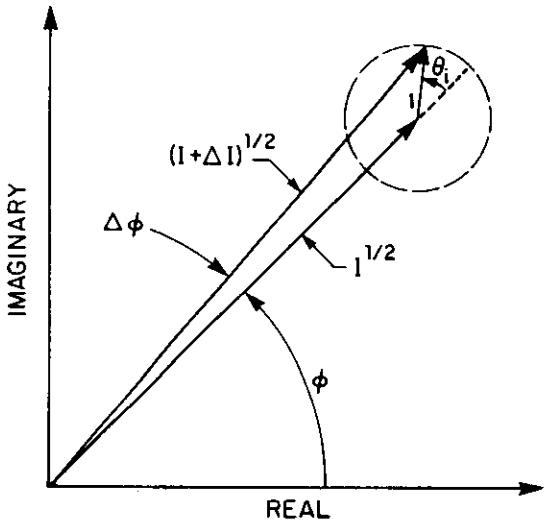

Fig. 1. Representation of the laser field in the complex plane with the proportionality constant in Eq. (1) set equal to one.

width of an LC triode oscillator was expressed as a function of the circuit parameters. This treatment can be extended[8] to account for the additional broadening mechanisms present in (GaAl)As type lasers. The differential equation describing the response of a noise driven oscillator is given by[10]

$$\frac{\partial^2 E}{\partial t^2} + \frac{1}{\tau_c}\frac{\partial E}{\partial t} + \omega^2 E + \frac{1}{n_o^2}\frac{\partial^2 P}{\partial t^2} = N(t) \quad , \qquad (11)$$

where $N(t)$ is driving noise term, ω is laser frequency, τ_c is the cavity lifetime, and n_o is the refractive index which does not include contributions from interband transitions. The induced polarization, P, is given by

$$P = [\chi^{(1)} + \chi^{(3)}E^2]E \quad , \qquad (12)$$

where

$$\chi^{(3)} = \chi_r^{(3)} + i\,\chi_i^{(3)} \quad . \qquad (13)$$

The real part of $\chi^{(3)}$ is due to index saturation while the imaginary part of $\chi^{(3)}$ is due to gain saturation. The results of this approach are essentially the same as those of Henry.

Phase Noise Sidebands

The spectral lineshape has, until recently, been considered to be Lorentzian. Osterwalder and Rickett[11] first reported the observation of sidebands associated with each longitudinal mode of a multimode (GaAl)As diode laser with an intensity of a few percent of the central peak and a frequency shift of 1-2 GHz. Recently, Daino et al.[12] and later Vahala et al.[13] have made more careful studies of this effect on single-frequency devices and explained the occurrence of these sidebands as due to a peak in the phase noise spectrum at the relaxation frequency. Henry[14] has presented a comprehensive theory of these sidebands which is derived from his initial treatment of the enhanced laser linewidth due to intensity fluctuations.

By referring to Fig. 1 it is easy to see that the perturbed laser field, $I+\Delta I$, will return to its average value I after undergoing damped relaxation oscillations. A delayed phase change will occur during these damped relaxation oscillations. The modulation of both the intensity and phase will therefore produce sidebands at the relaxation frequency. These sidebands have been observed[13] to increase in frequency and decrease in amplitude as the power is increased.

Power Independent Broadening

An additional line broadening has been observed[15,16] which has not been included in previous treatments and is discussed below. This is a power-independent contribution to the linewidth which has been described phenomenologically as due to refractive index fluctuations resulting from the statistitical fluctuations in the number of conduction electrons in the small active gain volumes of (GaAl)As diode lasers. Typical gain volumes for such lasers are $200 \times 2 \times 0.2$ μm.

The frequency of laser oscillation can be written as

$$\nu = (\nu_c\Gamma_g + \nu_g\Gamma_c)/(\Gamma_c + \Gamma_g) \quad , \qquad (14)$$

where ν_c is the cavity mode frequency, ν_g is the gain peak frequency, and Γ_c and Γ_g are the spectral half-widths of the passive cavity mode and the gain spectrum, respectively. The cavity mode frequency fluctuations are related to changes in the refractive index via the phenomenological relation

$$\delta\nu_c = (\nu_c/n)(dn/dN)_{N_t\nu}\,\delta N \quad , \qquad (15)$$

where δN is the mean square fluctuation in the number N of the electrons in the gain volume and dn/dN is evaluated at the laser frequency and at N equal to the number of electrons at laser threshold, N_t. For most cases of interest, the mean square fluctuation in electron number is assumed to be

$$\delta N = \sqrt{N_t} \quad . \tag{16}$$

The resulting expression for the laser frequency fluctuations is given by

$$\delta\nu = (\nu_c M \sqrt{N_t}/n)(dn/dN)_{N_t} \nu \, [\Gamma_g/(\Gamma_q+\Gamma_c)] \quad , \tag{17}$$

where M is a mode confinement factor which determines the fraction of the optical cavity frequency affected by index changes and is given by the ratio of cross-sectional optical mode area to carrier confinement area. The presence of the laser field will strongly damp the gain at high power levels and no carrier density fluctuations at frequencies less than the damped relaxation rate should be expected.

Fluctuations in the peak of the gain spectrum center frequency with electron number can also contribute to the linewidth when the carrier distribution becomes degenerate at low temperatures. Assuming that the terminal states for the lasing process are empty, the worst case is given by

$$\delta\nu = (2RE_{FC}/3\sqrt{N}) \, [\Gamma_c/(\Gamma_c+\Gamma_g)] \quad , \tag{18}$$

where R is a factor which accounts for the effects of band gap renormalization and is about 0.6 for (GaAl)As devices. The frequency change associated with this effect is of the same sign as the effects of Eq. (17).

An alternative model of the power-independent broadening has been presented by Vahala and Yariv[17] involving electron occupation fluctuations. This model does not require a change in electron number but depends upon the thermal fluctuations of electrons of order kT around the quasi-Fermi surface to produce a refractive index fluctuation at the laser frequency. The expression for the power-independent linewidth can be calculated using the formulation of Eq. (2) to get

$$2\Gamma = \frac{kT}{V}\left(\frac{\pi\omega AM}{n_0^2}\right)^2 \int_{-\infty}^{\infty} D(\Omega)\left(\frac{\omega-\Omega}{(\omega-\Omega)^2+1/T_2^2}\right)^2$$

$$\times \, [T_c(\partial f_c/\partial E_{FC})+T_v(\partial f_v/\partial E_{Fv})]d\Omega \quad , \tag{19}$$

where V is the gain volume, A is proportional to the matrix element, M is the mode confinement factor, $D(\Omega)$ is the reduced density of

states, T_2 is the dephasing time, T_c and T_v are the intraband relaxation times, f_c and f_v are the conduction and valence band occupation probabilities, and T is the absolute temperature. Many of the parameters in this model are not determined to a high degree of accuracy including the use of the Kane band structure matrix element. The intraband scattering times T_c and T_v are determined from mobility measurements[18] on different device structures and may not be the exact values operative in the semiconductor lasers. In any event, T_c and T_v would be expected to increase only slowly below 80 K resulting in Eq. (19) approaching zero as the temperature went to zero. This is in contrast with the experimentally measured[19] power independent broadening for TJS and CSP lasers at liquid helium temperature described below.

EXPERIMENTAL RESULTS AND COMPARISON WITH THEORY

Power-Dependent Broadening

The power-dependent linewidth of various types of (GaAl)As semiconductor lasers have been measured experimentally and compared with theory.[20] Experiments were carried out as a function of power and temperature on single-frequency channel-substrate planar (CSP) Hitachi and transverse-junction stripe (TJS) Mitsubishi diode lasers which operated continuously at room temperature. All devices which were measured operated with their output in a single frequency with "kink-free" power versus current at all temperatures. An example of the power versus current curves are shown in Fig. 2 for a Mitsubishi TJS device. In addition, measurements were made with the laser mode frequency tuned near the center of its tuning range to prevent mode hopping instabilities which would have a tendency to broaden the output line.

The devices were thermally isolated in a Dewar to reduce temperature instabilities to an insignificant level and to operate at reduced temperatures. Precautions were taken to prevent optical feedback by optically isolating the diodes. Injection current noise was also minimized by using a shielded lead-acid battery together with input filters. Later experiments were carried out with a special temperature controller and stable electronic power supply to eliminate long term drift effects.

Initial lineshape measurements were made using an external cavity, single-frequency (GaAl)As diode laser of < 15 kHz linewidth(21) heterodyned with the monolithic diode lasers. The same external cavity device was also used to determine the resolution of a scanning Fabry-Perot interferometer used for most other measurements. Frequency calibration of these instruments were also made by producing modulation sidebands on the monolithic devices with a precision frequency oscillator. The measurements produced similar results for all the devices studied, independent of the fabrication technique.

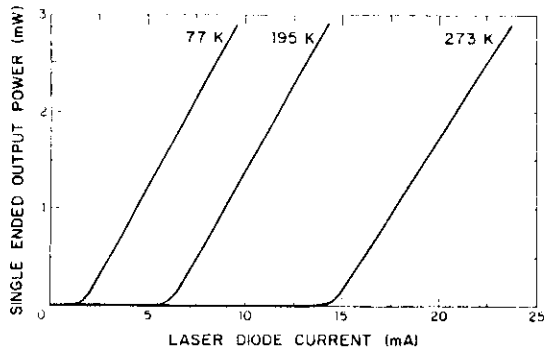

Fig. 2. Single-ended output power versus current for a Mitsubishi TJS diode laser at 273, 195, and 77 K.

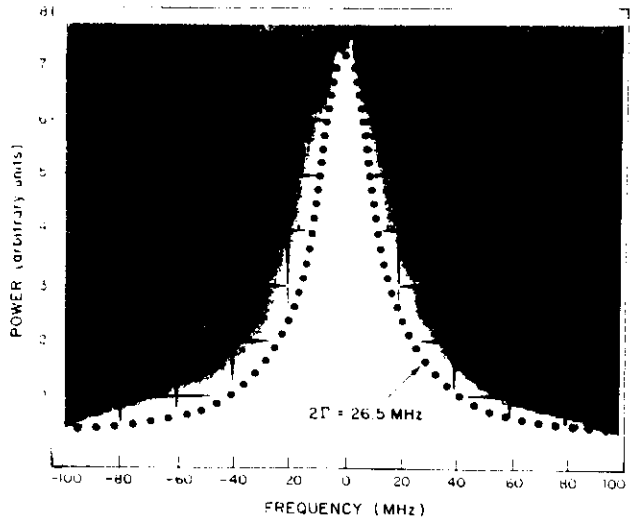

Fig. 3. Heterodyne beat spectrum between an external cavity (GaAl)As cw diode laser and a monolithic Hitachi CSP diode laser at 20 C. Fit is to a Lorentzian.

Figure 3 shows the spectrum of a monolithic diode laser heterodyned with a stable external cavity laser. The lineshape of the monolithic device was determined to be approximately Lorentzian and the linewidth was equal to that measured by the Fabry-Perot interferometer.

The laser linewidth as a function of reciprocal output power is shown in Figs. 4a, b and c at temperatures of 273, 195 and 77 K, respectively for a Mitsubishi TJS device. The linewidth is seen to decrease linearly with reciprocal output power as predicted by Eq. (4). In addition, there is seen to be a finite intercept which increases as the temperature decreases. This power independent contribution to the linewidth is attributed to electron number fluctuations described by Eq. (17). The linewidth versus reciprocal power for a Hitachi CSP laser is shown in Fig. 5.

In order to compare experiment with theory, the linewidth must be expressed in terms of the experimental parameters to give

$$2\Gamma = (h\nu/8\pi P_0)(c/nL)^2(\ell nR-\beta L)(\ell nR)n_{sp}(1+\alpha^2) \qquad (20)$$

where P_0 is the single-ended output power. The loss coefficient β was determined from the slope efficiency for each device measured. The parameter α was determined from measurements of $\Delta\lambda$ and Δg with current. Because of the approximate linearity of $\Delta\lambda$ and Δg with electron density for the experimental condition of a near-degenerate conduction band and a highly degenerate valence band, as is the case for the devices discussed here, changes of laser mode wavelength and gain integrated over a change in carrier density from zero injection current to threshold should give a reasonable estimate for α, as only the ratio of these parameters enters. The spectral shift of the Fabry-Perot laser mode center frequency as a function of injection current up to threshold was used to estimate $\Delta\lambda$. The thermal contribution to the spectral shift is approximately an order of magnitude smaller than that due to carrier density variation, in contrast to lead-salt lasers, and can be neglected in the estimation of $\Delta n'$. The laser output power versus injection current was used to estimate the change in gain for a change of carrier density from zero injection current up to threshold.

At 273 K, for example, the calculated change in gain up to threshold is 133 cm^{-1} and the spectral shift of the laser mode extrapolated from threshold to zero injection current gives an observed $\Delta\lambda$ of -8.1 Å. Using Eqs. (9) and (10) gives a value of 15.5 for $(1+\alpha^2)$. The inverse power dependence ofthe linewidth is then calculated to be 67.2 MHz mW which compares to the least square fit to the data of 74.7 MHz mW. Table I shows the parameters which were measured and the related theoretical estimates. It is important to note that parameter values for different devices fabricated the same way can vary sufficiently to require their determination for each comparison between experiment and theory. Such variations can change

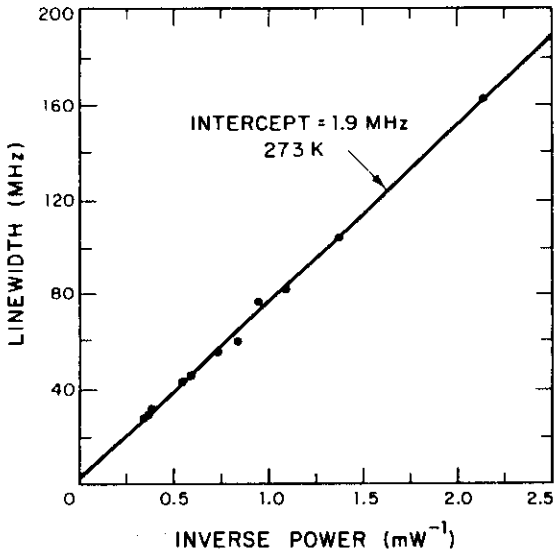

(a)

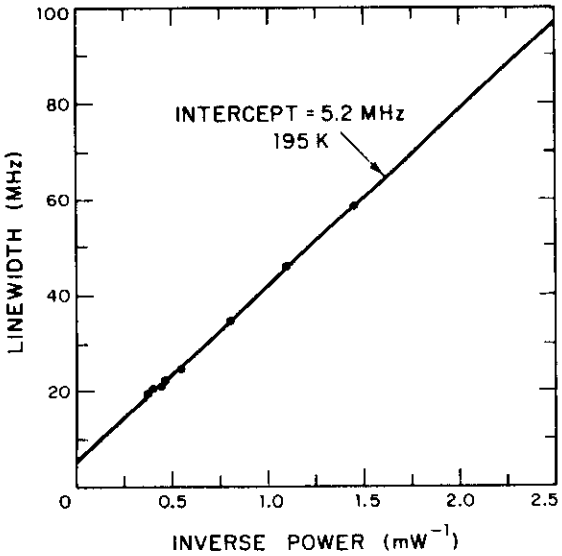

(b)

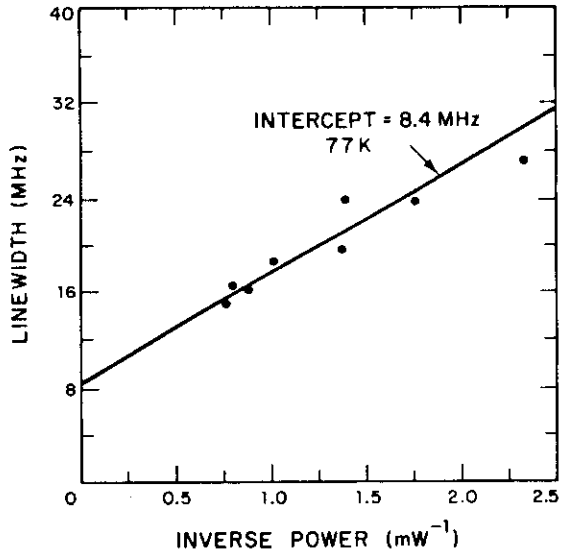

(c)

Fig. 4. Linewidth of a Mitsubishi TJS diode laser as a function of the inverse of the single-ended output power at three temperatures: (a) 273 K, (b) 195 K, and (c) 77 K.

the observed linewidth for a given power level by as much as 10-20 percent. A significantly larger variation between devices made by different technique can occur as is seen in the comparison between Figs. 4 and 5.

Power Independent Broadening

For the power independent contribution to the laser linewidth, the change of refractive index at N_t with electron number was determined by monitoring the spectral shift of the Fabry-Perot modes as a function of injection current up to laser threshold. Typical data are shown in Fig. 6 for the spectral mode shift at 195 K. The rate of change of refractive index is expected to be linear with carrier density. The relation between carrier density and injection current, however, is parabolic[22] up to threshold which causes the parabolic shift of mode frequency with injection current. The parameter M in Eq. (17) is estimated to be ~ 0.4 for TJS devices, and the factor $\Gamma_g/(\Gamma_c+\Gamma_g)$ is approximately unity. Table II

Table I. A summary of measured device data and theoretical estimates of the power-dependent linewidth contribution for Mitsubishi TJS diode lasers.

	77 K	195 K	273 K
λ(nm)	803	824	842
$\Delta\lambda$(A)	-2.6	-6.0	-8.1
Wg(cm^{-1})	88.3	100	133
n_{sp} (calculated)	1.12	1.69	2.12
$(1 + \beta^2)$	5.1	16.4	15.5
Theoretical estimate of $2\Gamma P_0$ (MHz mW)	8.2	43.7	67.2
Experimental observation of $2\Gamma P_0$ (MHz mW)	9.28	36.7	74.7

Table II. A summary of measured device data and theoretical estimates of the power-independent linewidth contribution for Mitsubishi TJS diode lasers.

	77 K	195 K	273 K
λ(nm)	803	824	843
I_t (mA)	1.3	6.3	13.5
N_t	1.7×10^7	8.4×10^7	1.8×10^8
$(\partial n/\partial N)_{N_t \nu}$	8.4×10^{-11}	2.2×10^{-11}	5.2×10^{-12}
$2\Gamma_{theory}$ (MHz)	11.5	6.5	2.2
$2\Gamma_{exp}$ (MHz)	8.4	5.2	1.9

summarizes the experimental parameters and the comparison between experiment and theory at three temperatures.

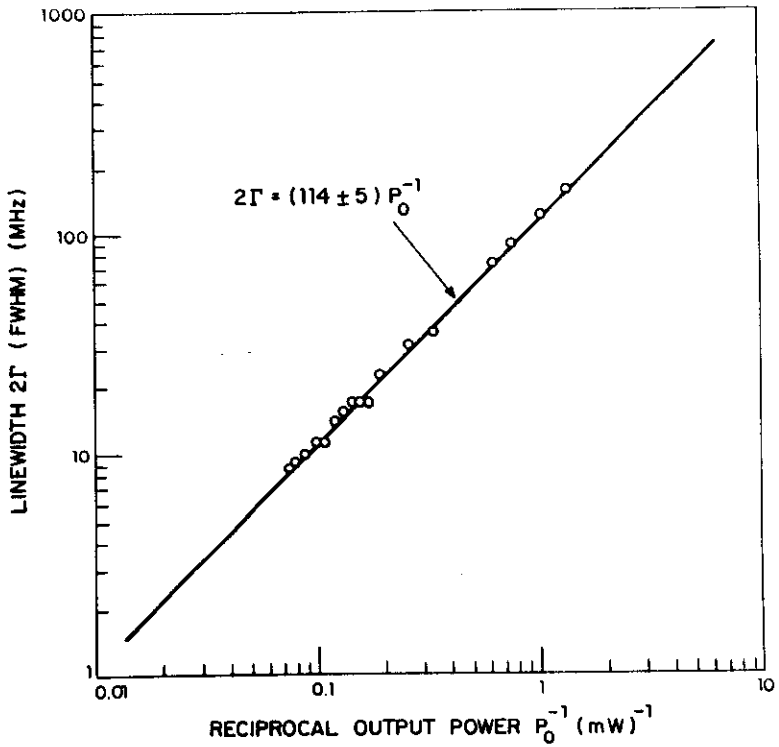

Fig. 5. Linewidth of a Hitachi CSP diode laser at 0 C as a function of the inverse of the single-ended output power. The slope is 114 ± 5 MHz with an infinite power intercept of 2.7 ± 0.8 MHz. Mean variance of data is ± 1.5 MHz for output powers greater than 2 mW.

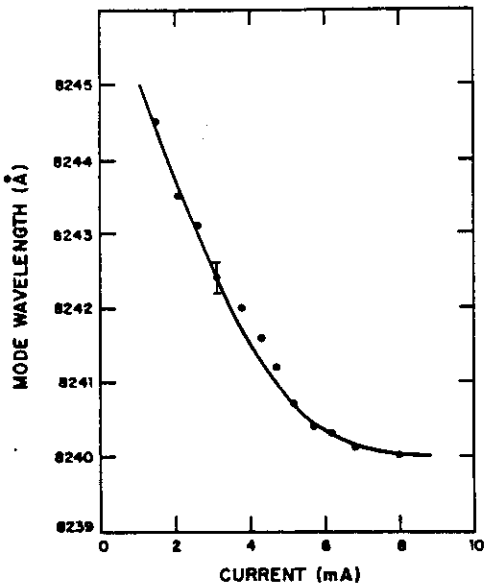

Fig. 6. Shift of the Fabry-Perot laser cavity peak wavelength at the laser frequency for a Mitsubishi TJS laser at 195 K.

The contribution to the power independent linewidth due to fluctuations in the peak of the gain spectrum center frequency with electron number fluctuation becomes significant only at low temperature and would be no more than a few MHz for temperatures below about 20 K. In addition to the data shown in Table II, measurements[23] made at liquid helium temperature (Fig. 7) indicates a power independent broadening value of about 30 MHz which is also consistent with the greatly reduced threshold currents and increased value of resonant dispersion. This behavior is in agreement with the phenomenological power-independent broadening model of ref. (16) and the power-dependent theory of ref. (8). This is in apparent contrast with the predictions of the Vahala and Yariv[17] theory in which the linewidth of Eq. (19) approaches 0 as $T \to 0$. The exact origin of the fluctuations is not clear. However, it appears that this broadening may be related to the presence of 1/f noise[24] in the device.

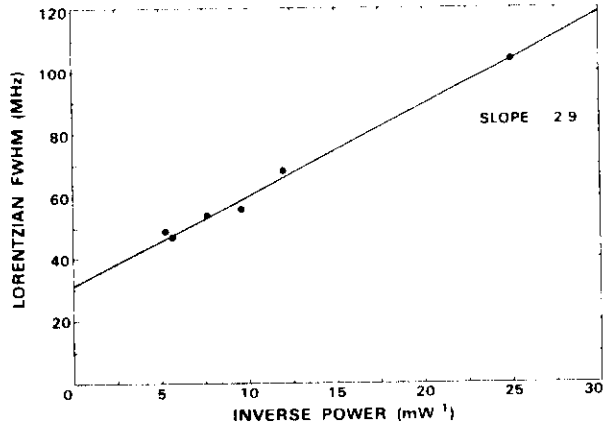

Fig. 7. Linewidth of Mitsubishi TJS laser at 1.7 K.

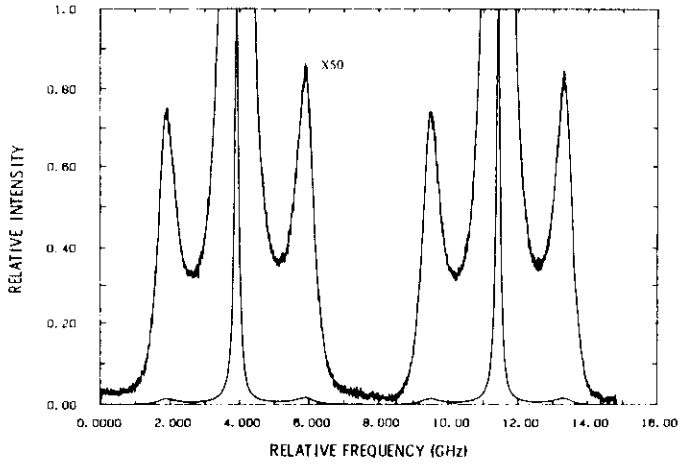

Fig. 8. Fabry-Perot trace of the output of a Hitachi CSP diode laser at 20 C showing relaxation resonance sidebands. Resolution of Fabry-Perot was 35 MHz. Single-ended output power of diode laser was between one and two milliwatts.

It is interesting to note that the power independent contribution to the laser linewidth is a dominant broadening mechanism at high output power levels at room temperature and at most power levels at low temperature. This effect limits the usefulness of these devices for many high resolution applications but it can be overcome by use of an external cavity as described in the next section. The implications of this power independent broadening mechanism are most significant as device structures become even smaller.

Phase Noise Sidebands

The sidebands at the relaxation frequency described above are shown experimentally[25] in Fig. 8. The magnitude of the frequency shift has been observed to vary as the square root of the power in the main laser mode in agreement with the dependence of the relaxation oscillation frequency with stimulated emission rate. The intensity of these sidebands linearly decrease in magnitude with increasing laser mode intensity.

EXTERNAL CAVITY (GaAl)As LASERS

This section describes the spectral characteristics of (GaAl)As diode lasers operated in external cavity structures. Use of an external cavity can overcome many of the spectral limitations described in the preceding sections and provide a device with a very narrow linewidth and controlled tuning characteristics. A disadvantage of an external cavity structure is the greater complexity of a hybrid structure over a monolithic device. With advances in fabrication of small optical components, this does not turn out to be a significant disadvantage. In fact, considering the hybrid technology of fiber optical connectors and transmission systems in general, the new generation miniature external cavity devices are quite reasonable.

The CSP and TJS lasers described in the previous sections operate with nearly all of their output power in a single frequency in contrast to earlier generation devices which had a multi-longitudinal mode output even when they operated in what appeared to be a single spatial mode. These early lasers were of the wide stripe design (i.e., greater than 10 μm junction width) which for a typical cavity length of 200 to 300 μm meant a Fresnel number of greater than one. The narrow stripe width (~ 1-2 μm) of the CSP and TJS lasers has led to single-frequency operation in part because these lasers have a Fresnel number near unity; however, the actual device fabrication technique strongly contributes to the mode structure. The subject of multi-longitudinal mode operation of diode lasers which presumably operate in a single spatial mode has been discussed but not completely understood for some time. Recently, Liu et al.[26] have studied the intensity statistics of diode lasers in which the output occurred in a predominantly single mode. It was found that a weaker adjacent longitudinal mode could for a short period of time increase in power

a predominantly single mode. It was found that a weaker adjacent longitudinal mode could for a short period of time increase in power to the power of the main mode, whilethat main mode power decreased in intensity so that the total power remained constant.

Use of an external cavity to force oscillation in a single fundamental spatial mode[21] for a diode laser which would normally operate with many longitudinal modes had the effect of producing a single-frequency output with nearly all of the double-ended multimode power of the diode laser before it was operated in the external cavity. Figure 9 shows a typical multimode output spectrum of a (GaAl)As diode laser operating continuously at room temperature. These lasers were antireflection coated on both ends so that no laser action would occur at the maximum injection current levels used before coating. Figure 10 shows the output spectrum from this device when operated within an external cavity as shown schematically in Fig. 11. Similar results were repeatedly obtained with several dozen such lasers. By use of very wide junction lasers it would be possible to extract a few hundred milliwatts of continuous output power at room temperature from one diode laser in a single, stable frequency and one or more watts of power at low temperature.

It is important to note that when a normally multimode device is forced to oscillate in a truly single spatial mode, nearly all of the multimode output can be extracted in a single frequency. This has been demonstrated in an external cavity structure even when operated without a tuning element in the cavity.[19] This implies that there exists neither spectral nor spatial hole burning in these lasers.

Spatial hole burning, a common source of multi-longitudinal mode operation in many lasers, occurs when the local field intensity of the standing wave in the laser cavity saturates the local population inversion. The adjacent cavity mode of next order will not overlap in the center of the cavity and can be sustained because the population inversion is localized. In the case of a semiconductor laser, the inversion is from mobile carriers and any hole burning will be washed out due to thermal diffusion. The time for thermal diffusion over a distance of about one quarter of the wavelength of the standing wave in the material (several hundred A) is comparable or faster than the stimulated emission rate.

Spectral hole burning is a second source of multi-longitudinal mode operation in lasers with inhomogeneous gain broadening. For interband transitions in materials such as (GaAl)As, most of the transitions are direct with only removal of the k selection rule near the band edge for the doping levels (~ 10^{18} cm^{-3}) typically encountered in these devices. At room temperature, phonon scattering as well as carrier-carrier scattering produce an intraband scattering time on the order of 10^{-13} sec as determined from traditional methods. Figure 12 shows the interband laser transition

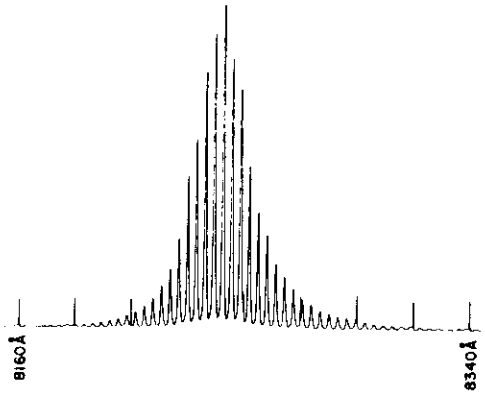

Fig. 9. Emission spectrum of cw room temperature (GaAl)As diode laser before operation in external cavity.

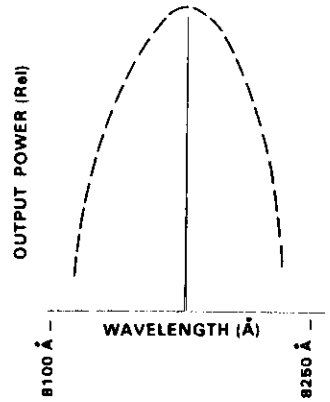

Fig. 10. Spectrometer trace and tuning range of a grating controlled external cavity (GaAl)As diode laser operating cw at room temperature. Maximum output power was several milliwatts.

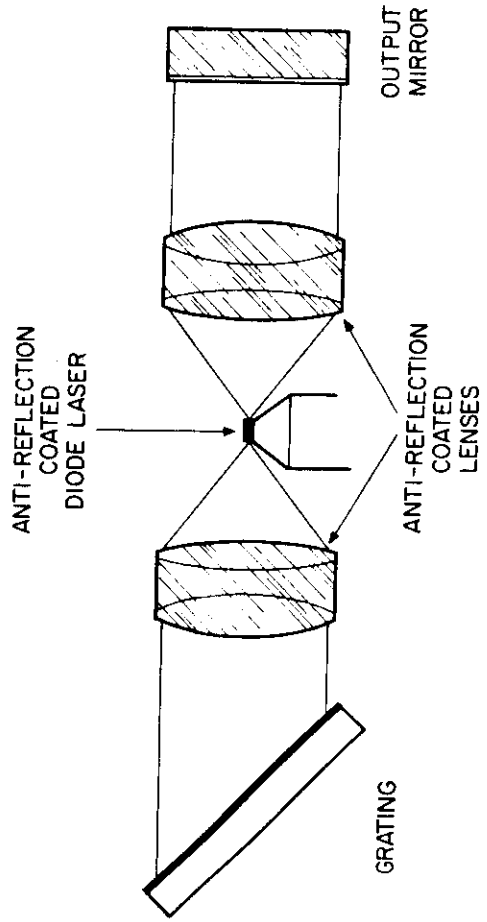

Fig. 11. Schematic diagram of a double-ended external cavity diode laser.

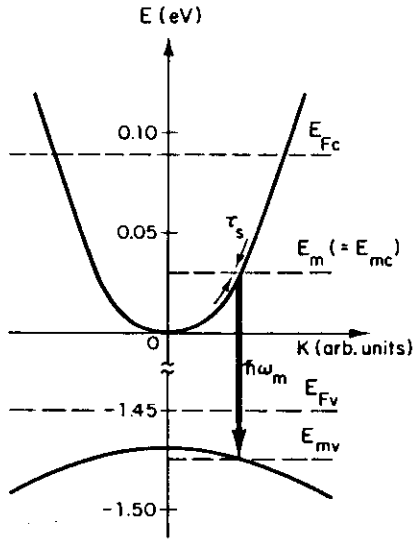

Fig. 12. Schematic diagram of the simplified band structure of (GaAl)As showing the direct interband laser transition.

while Fig. 13 shows schematically the hole which would be formed in the electron distribution function and the corresponding effect on the spontaneous emission emitted from the recombination of carriers in the gain region. Because of the large hole effective mass, valence band hole burning effects can be neglected. Calculated hole widths[12] for an intraband scattering time of 10^{-12} and 10^{-13} s are 1.3 and 13 meV, respectively. Corresponding hole depths are 4×10^{-3} to 4×10^{-5} of the peak of the luminescent intensity at the laser frequency.

An attempt has been made to measure the hole burning on a (GaAl)As diode laser[21] using an external cavity device. By observing the luminescent emission along the axis of the laser it was possible to externally aperture the beam and observe only the emission coming from the mode volume of the laser where hole burning would be expected to occur. Figure 14 shows the results of experiments performed on an external cavity device operating witha one milliwatt output power compared with theoretical calculations of the effects of a hole burned with a one percent depth. No holes were observed

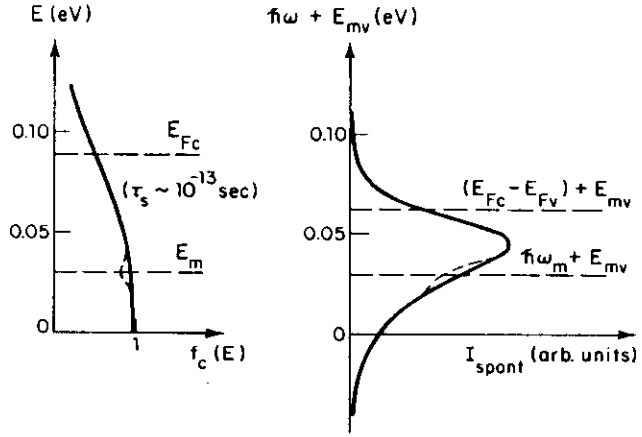

Fig. 13. Representation of hole burned into electron distribution function and corresponding hole as it would appear on the electron-hole recombination spectrum.

to the sensitivity limit of about 0.5% of the intensity of the luminescent intensity indicating that the intraband scattering time would be faster than about 5×10^{-13} sec according to existing models.[21] This is consistent with the fact that the external cavity as well as monolithic CSP and TJS type lasers operate in a single axial mode.

The limitations imposed by the fundamental linewidth broadening mechanisms described in Section II can be overcome by the use of an external cavity. The linewidth will be narrowed by the square of the ratio of the relative cavity lengths when the unloaded cavity length is significantly larger than the length of the diode. Figure 15 demonstrates the narrow linewidth that can be achieved[15] using an external cavity structure heterodyned together. The observed linewidth of 30 kHz implies that the linewidth for each of the lasers is less than 15 kHz. This is for the case of two Lorentzian lines. The expected fundamental linewidth for each of the lasers in this experiment at their output power levels would be about 400 Hz. The measurement limitation was set by the RF spectrum analyzer. With present technology, it should be possible to construct a small external cavity device with a fundamental width of about one hertz and an unlocked jitter width of a few kilohertz.

The amplitude noise spectrum is shown in Fig. 16 from essentially dc to 2 GHz. Only slight traces of 120 Hz and an external

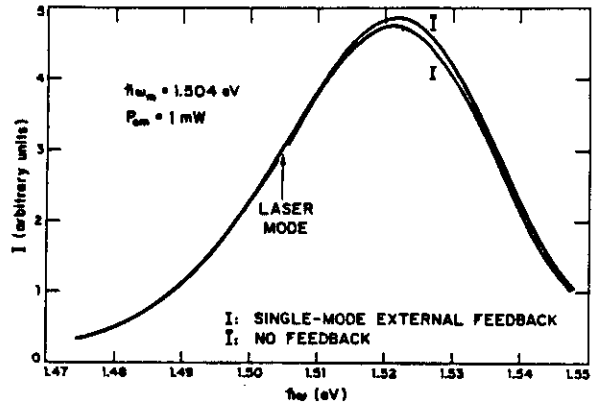

(a)

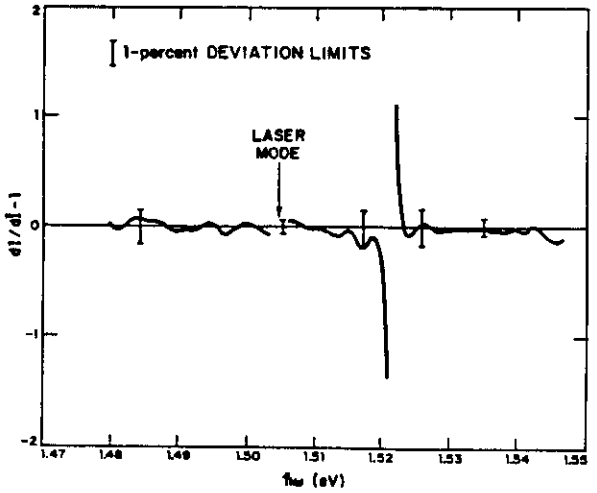

(b)

Fig. 14. (a) Spontaneous emission spectrum from (GaAl)As room temperature external cavity laser with and without feedback. (b) Spectrum of the ratio of the energy derivatives of the lasing and nonlasing spectra in (a).

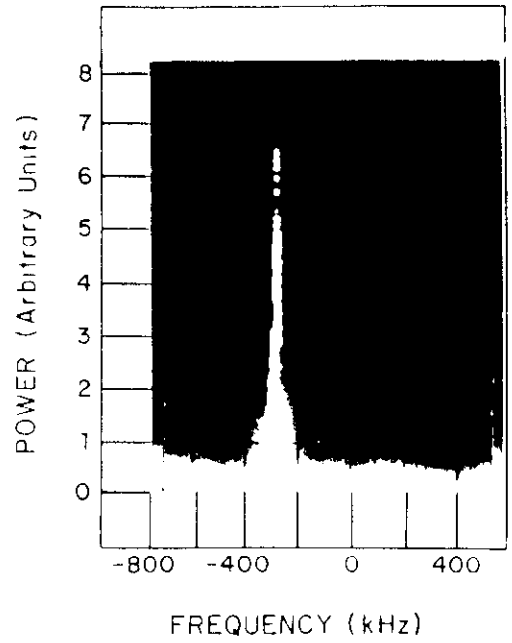

Fig. 15. Heterodyne beat spectrum between two spectral cavity (GaAl)As cw diode lasers at 850 nm with output powers of 0.4 and 0.34 mW, respectively.

cavity relaxation resonance at 25-40 MHz can be seen. A smaller and simpler external cavity structure would eventually have very high amplitude and phase stability making it an ideal source for metrological applications.

External cavity lasers have gone through various stages of evolution and like many other types of laser devices, they must be in a reasonably stable cavity structure in order to examine many of their interesting physical properties. An intermediate design is shown in Fig. 19 in which a Hitachi CSP diode laser having both ends antireflection coated is in a stable cavity employing a microscope objective lenses. Most of this structure is fabricated from Invar for stability. With the very low (< 0.3%) reflectivity coatings presently possible for (GaAl)As diode lasers, a greatly simplified cavity design using only one microscope objective lens with the diode

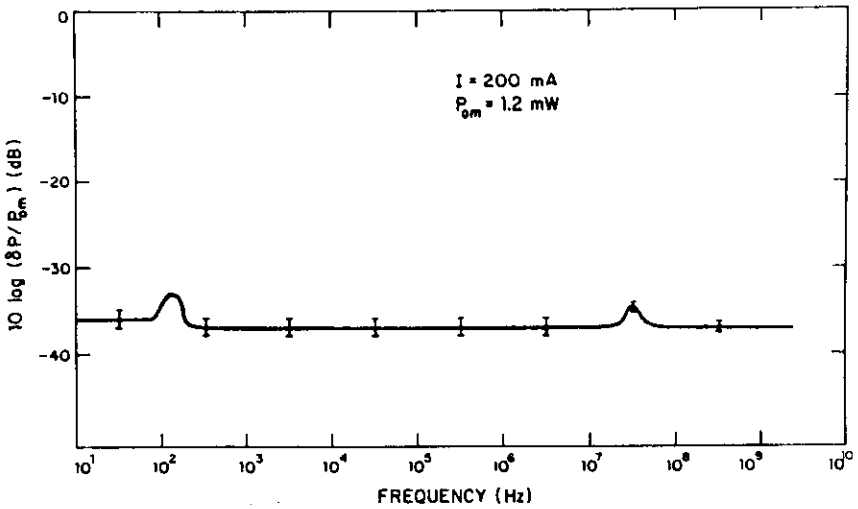

Fig. 16. Laser intensity noise spectrum detected in a bandwidth of 10 Hz over the frequency range 10 Hz to 100 kHz, 100 Hz from 100 kHz to 1 MHz, 10 kHz from 1 MHz to 10 MHz, and 100 kHz from 10 MHz to 2 GHz. The spectra are essentially flat in each frequency interval and are therefore joined continuously for this complilation. The magnitudes of the noise peaks must be divided by the corresponding bandwidths for quantitative comparison. The power scale is normalized to the average mode intensity for a 10-Hz detection bandwidth. Error bars indicate the average scatter in the recorded spectra over the component frequency ranges. The peak at 120 Hz is due to power supply ripple while the peak in the range 25-40 MHz is due to relaxation oscillations of the external cavity.

antireflection coated on one side and 100% reflectivity coated on the other side allows the use of simple, commercially available diode lasers. Commercially available microscope objective lenses do not have significant loss at typical (GaAl)As diode laser wavelengths and can be used in a simple rigid cavity design with a significantly larger volume-to-surface ratio than previous designs. A very compact, stable, external-cavity device which is also relatively inexpensive

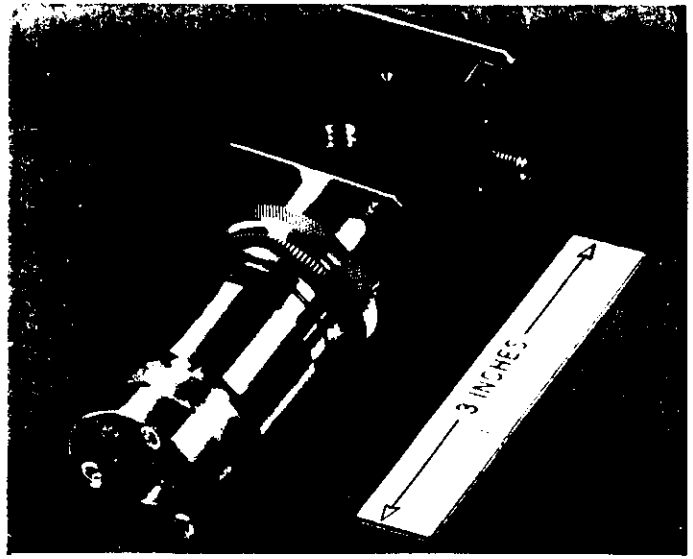

Fig. 17. Photograph of a stable external cavity (GaAl)As diode laser.

can be fabricated for various applications in high resolution spectroscopy, short-pulse generation, and optically pumped frequency standards.

REFERENCES

1. M. Lax, Phys. Rev. 160, 290 (1967).
2. A. L. Schawlow and C. H. Townes, Phys. Rev. 112, 1940 (1958).
3. C. H. Henry, R. A. Logan, and K. A. Bertness, J. Appl. Phys. 52, 4453 (1981).
4. M. W. Fleming and A. Mooradian, Appl. Phys. Lett. 38, 511 (1981).
5. M. Lax, Phys. Rev. 157, 213 (1967).
6. H. Haug and H. Haken, Z. Physik 204, 262 (1967).
7. C. H. Henry, IEEE J. Quantum Electron. 18, 259 (1982).
8. K. Vahala and A. Yariv, IEEE J. Quantum Electron. 19, 1096 (1983).
9. M. Sargent, M. O. Scully, and W. Lamb, Jr., in Laser Physics (Addison-Wesley Publishing Company, Reading, Massachusetts, 1974).
10. Y. Yamamato, IEEE J. Quantum Electron. 19, 34 (1983).
11. J. M. Osterwalder and B. J. Rickett, Proc. IEEE 67, 1671 (1979).
12. B. Daino, P. Spano, M. Tamburrini, and S. Piazzola, IEEE J. Quantum Electron. 19, 266 (1983).
13. K. Vahala, Ch. Harder, and A. Yariv, Appl. Phys. Lett. 42, 211 (1983).
14. C. H. Henry, IEEE J. Quantum Electron. (to be published).
15. A. Mooradian, D. Welford, and M. W. Fleming, in Proceedings of Fifth-International Conference on Laser Spectroscopy, Jasper, Canada, 1981, edited by A. R. W. McKellar, T. Oka, and B. P. Stoicheff (Springer-Verlag, 1981), p. 67.
16. D. Welford and A. Mooradian, Appl. Phys. Lett. 40, 560 (1982).
17. K. Vahala and A. Yariv, Appl. Phys. Lett. 43, 140 (1983).
18. H. L. Stoumer, A. Pinczuk, A. C. Gossard, and W. Wiegmann, Appl. Phys. Lett. 38, 691 (1981).
19. Measurements by J. Harrison and A. Mooradian.
20. D. Welford and A. Mooradian, Appl. Phys. Lett. 40, 865 (1982).
21. M. W. Fleming and A. Mooradian, IEEE J. Quantum Electron. 17, 44 (1981).
22. S. E. H. Turley, G. H. B. Thompson, and D. F. Lovelace, Electron. Lett. 15, 256 (1979).
23. J. Harrison and A. Mooradian, Appl. Phys. Lett. 45, 318 (1984).
24. K. Kikuchi and T. Okoshi, Electron. Lett. 19, 813 (1983).
25. Measurements by J. Harrison and A. Mooradian.
26. P. L. Liu, L. E. Fencil, I. P. Kaminow, T. P. Lee, and C. A. Burrus, to be published in IEEE J. Quantum Electron.

ADVANCES IN SOLID STATE LASER TECHNOLOGY AND APPLICATIONS

A. Mooradian

MIT Lincoln Laboratory

INTRODUCTION

Within the next few years, nearly 70 percent of the entire laser market will be dominated by semiconductor lasers or laser arrays which will be used to pump other solid state lasers or will operate with a coherent output from a two dimensional array. Output powers in excess of one kilowatt with more than 10 per cent power efficiency should become commercially available. These lasers will provide a major boost for
industrial processing and medical applications. Recent advances in solid state and semiconductor lasers are discussed here.

Included is a description of work on phonon broadened laser devices using the crystal sapphire doped with titanium, diode pumped solid state lasers and ultrastable external cavity semiconductor diode lasers. All of these lasers have become important recently because of their broad range of tunability, efficient operation and all solid state operation which means that compact lasers can be made for reliable and rugged operation. Worldwide research has shifted in the direction of such technology in the past few years and will continue in the future. Many of these lasers are now commercially available throughout the world.

TITANIUM SAPPHIRE LASER

The titanium doped sapphire laser was first made to operate several years ago and has now become a commercially available device sold by a number of companies throughout the world. This laser is rapidly becoming a replacement for dye lasers which operate in the near infrared. They are usually pumped by cw argon lasers or frequency doubled Nd:YAG lasers. Figure 1 shows the spectral properties of Ti:sapphire indicating the broad absorption band in the visible region and the demonstrated range over which laser action has occurred. This range is from 660 nm to nearly 1100 nm. The second figure shows a an example of a boule of Ti:sapphire of the type which is now commercially available from such companies as Union Carbide or Crystal Systems in the USA. This material in its best form has a broadband residual absorption which occurs in the laser gain region of less than one percent of the peak absorption of the main pump band at 500 nm. Figure 2 show a photograph of two Ti:sapphire crystals which were grown by a modified Bridgeman technique. Lasers which have been fabricated from Ti:sapphire have been operated in a number of configurations in various laboratories around the world. Continuously operated devices pumped by an argon ion laser have produced over several watts of output power at room temperature. Pulsed lasers have operated using flashlamps as well as high-energy frequency doubled Nd:YAG laser radiation. In addition, a high rep-rate Q-switched and frequency doubled Nd:YAG laser has been used to generate a single gain

switched spike from a Ti:sapphire laser having a pulse width of 30-100 ns and a peak power of several kilowatts. In addition to the various pumping schemes, the Ti:sapphire laser has been operated in a single frequency as a ring laser. The characteristics of this laser are single frequency unidirectional output with a linewidth of less than 30 kHz. Most of these Ti:sapphire laser configurations are now commercially available.

OTHER SOLID STATE LASERS

Many sold state lasers have been developed over the past twenty years and a recent resurgence of interest has occurred in the past several years which has resulted in major advances in solid state laser technology. Listed below are several of these new laser materials with some of their relevent laser properties.

MATERIAL	*CHARACTERISTICS*
Garnets GSGG,GGG Doped with Nd, Cr etc.	Efficient energy transfer from Cr to Nd. Also Cr transitions are broad
Fluorides doped with transition metal ions such as Ni, Co, etc.	Broadband tunable 1 - 2.5 μm region
Stoichiometric compounds such as Nd pentaphosphate	High density of Nd with full spectral properties
Titanium doped sapphire and similar structures	Tunable near IR and visible lasers
Color centers in numerous host crystals	Tunable from visible out to 4 μm

As one example of the demonstrated operating characteristics of a tunable solid state laser in the Cobalt doped Magnesium Fluoride laser. This laser has been pumped by a 1.3 μm output from a Nd:YAG laser and the properties are listed below.

TUNING RANGE	1.55 - 2.4 μm
OUTPUT POWER	> 5 W CW
OUTPUT ENERGY	
Pulsed	> 200 mj
Q - switched	> 100 mj in one μs
MODE - LOCKED	
Pulse width	20 - 70 ps
Average power	> 2 W
OPERATING TEMPERATURE	TYPICALLY 77 K 300 K Pulsed

The cobalt doped magnesium fluoride laser is now commercially availble.

EXTERNAL CAVITY DIODE LASERS

Monolithic diode lasers which operate without an external cavity have spectral linewidths that are typically 30 MHz at output power levels of about 10 mW. Such spectral linewidths are not useful for a wide range of applications such as radar, optical heterodyne communications and high resolution spectroscopy. The source of the spectral broadening in these semiconductor diode lasers is fundamental and quantum in nature and arises from the spontaneous emission noise within the laser. This spontaneous emission noise causes the phase of the electric field vector of the radiation to fluctuate which in turn leads to a spectral broadening. In addition, damped relaxation oscillations which come about when the field amplitude is also perturbed by the spontaneous emission noise causes sidebands to occur which are typically 1-2 GHz away from the main peak. When such devices are placed into high Q external cavities, the linewidths are significantly reduced. Figure 3 show a photo of an ultrastable external cavity dioe laser. Linewidths of less than 400 Hz have been produced in such lasers. Figure 4 shows the spectral output of a single mode monolithic GaAlAs diode laser taken using a Fabry-Perot interferometer. A spectral width of about 30 MHz is seen together with the relaxation sidebands. The trace on the right is a heterodyne beat signal between two free-running external cavity lasers shown on a logarithmic scale using diode lasers which are nearly identical in construction to those for the left hand side of the figure. The linewidth in this case is only a few kHz. Figure 5 shows the heterodyne beat signal on a linear scale for a fast scan of 30 ms and for a slow scan of 60 s This demonstrates the various components which contribute to the frequency fluctuation spectrum of these stable external cavity lasers. The short term and long term fluctuations are on the order of several kHz and are starting to approach the fundamental kT noise of the resonator structure which are driven by phonon modes in the resonator material. This is a fundamental limit and can only be overcome by operating at a lower temperature or by locking the laser to some stable frequency reference. To demonstrate the ability to frequency stabilize these devices, an experiment was carried out in which one laser was frequency locked to another one which was free-running. The resulting heterodyne beat note with a 224 MHz offset is shown in Fig. 6. Here the scale is 10 Hz per division, indicating a narrow linewidth as well as a centroid frequency stability in the mHz range. By locking such a laser to a stable secondary standard, it would be possible to provide a very stable laser frequency standard with absolute frequency stabilities in the milliHertz region. Such devices could become very inexpensive and reliable sources for frequency standards. The frequency stability characteristics of free-running external cavity GaAlAs diode lasers which have already been demonstrated are listed below.

Fundamental width	< 1000 Hz
Future capability	< 10 mHz
Short term jitter	~ 5 kHz/30 ms
Long term jitter	~ 7 kHZ
Center frequency drift	~ 5 kHz/h
Locking stability	< 10 mHz

Baseband noise +/- 5 GHz	< 100 dB

Extending the useful frequency range of presently available diode lasers such as GaAlAs can be accomplished by the use of efficient nonlinear frequency conversion. Wide bandgap semiconductor diode lasers have been very difficult to operate at wavelengths shorter than 600 nm. The materials of choice would be the II-VI compounds but so far have not proven to operate as diodes because of the inability to fabricate p-type material. Therefore, nonlinear frequency conversion would be one solution for the near term operation of compact blue diode laser sources.

Major advances in high power diode lasers have been made in the world with the development of the GRIN-SCH (Graded Index Separate Confinement Heterostructure) GaAlAs diode laser. These lasers have produced over one watt of cw power at room temperature with more than 50% power conversion efficiency. Figure 7 shows the cw output from such a laser as a function of injection current. One problem with these monolithic devices is the poor spectral output. This may be improved by operation in an external cavity. Because the broadening mechanism in semiconductor lasers leads to a homogeneous gain line, all of the laser output will occur in a single frequency when the device is operated in a single spatial mode. Such a diode laser has been operated in an external cavity and has produced more than 1.5 watts of continuous power at room temperature in a spectral width of less than 8 GHz and a spatial beam quality which was better than 2-3 times diffraction limited. Because of the energy band properties of quantum well laser materials, the gain bandwidths can be very broad. A single such laser when operated in an external cavity with a grating has been continuously tuned from 790 to 860 nm at room temperature. Two such lasers have covered the range from 720 to 870 nm. Frequency doubling of such high power devices would produce useful radiation from 360 to 435 nm with additional tuning over the entire visible range possible by parametric conversion.

DIODE PUMPED SOLID STATE LASERS

The use of efficient diode lasers and diode laser arrays are now in widespread use as efficient pump sources for solid state lasers to provide all solid state, compact, reliable and efficient lasers which are able to produce outputs from a few mW to more than 100 W. Such lasers would find numerous applications where the disadvantages of lamp pumping are obvious. The most common material that has been pumped by diode lasers is Nd:YAG which has its main output lines at 1.06 and 1.32 μm.

Single-frequency, diode-pumped, solid-state lasers have been the goal of researchers over the past 20 years. Solid-state lasers normally have relatively large cavities, such that several cavity modes fall under the gain profile of the active medium. Intracavity frequency selective devices are usually required in order to obtain single-frequency operation. As laser cavities are made smaller, the longitudinal mode spacing of the cavities becomes larger, and for small enough cavity lengths only a single cavity mode can . In linear cavity designs, spatial hole burning still leads to the simultaneous oscillation of two longitudinal cavity modes at pump powers only slightly above threshold. An alternative approach is the unidirectional ring cavity which avoids spatial hole burning. While this approach provides the desired laser characteristics, it suffers from a complicated fabrication process and critical optical alignment.

Another desirable property of lasers is tunability. Tuning of large lasers is usually obtained by using a frequency selective device to go from one longitudinal cavity mode to another, and is therefore discrete. Alternatively, a change in optical length may be used to obtain continuous tuning of lasers. The tuning range available through this type of tuning is limited to the distance between longitudinal cavity modes, before a neighboring longitudinal mode is tuned into the region of highest gain. A third tuning technique is the modulation of the cavity length at very nearly (but not exactly) a multiple of the longitudinal-mode frequency interval of the laser cavity. Large amounts of continuous tuning may be obtained in this way, but only at well defined rates of modulation.

The microchip lasers are designed to be inherently single-frequency lasers. The cavity length of microchip lasers is chosen so that only a single longitudinal cavity mode falls under the gain curve. In this way, the microchip lasers are fundamentally different from other single-frequency lasers such as the stoichiometric Nd lasers and unidirectional ring lasers. Figure 8 shows the concept of the microchip laser. The single-frequency operation of the microchip lasers allows the potential for continuous tuning over the entire gain bandwidth of the laser by changing the optical length of the cavity. The geometry of the microchip cavity and the pumping configuration strongly favor the TEM_{00} transverse mode, and only one transverse mode oscillates. Since the two orthogonal polarization modes of the microchip lasers are for the same longitudinal and transverse mode, they compete for gain. The first polarization mode to lase depletes the gain for the second mode - spatial hole burning does not create favorable conditions for the second polarization mode to lase - and only one polarization mode oscillates.

Because of the short cavity length, microchip laser cavities can be flat-flat. As a result, the fabrication process for microchip lasers lends itself to mass production. Because of the small amount of material used for each laser, and the simple fabrication, the cost per laser is extremely low. Once created, microchip lasers can be pumped with commercially available diode lasers. Figure 9-10 show the small microchip crystals after having been cut from a large boule of YAG as well as a finished microchip laser made from Nd:YAG and pumped by a cw diode laser.

Several different microchip lasers were constructed and operated cw at room temperature. Initially, the lasers were created by polishing a piece of crystal flat-flat, and sandwiching the crystal between two mirrors. The mirrors were created by di- electrically coating 100-mm-thick glass wafers. The output mirror had a reflectivity of 99.7% at the lasing wavelength and was designed to reflect the pump laser. The opposite mirror had a reflectivity of 99.9% at the lasing wavelength and transmitted the pump. The lasers that were constructed in this way included: Nd:YAG ($Nd_xY_{3-x}AlO_{12}$) at 1.064 mm using a 730 mm long cavity; Nd:YAG at 1.319 mm using a 730-mm-long cavity; Nd pentaphosphate (NdP_5O_{14}) at 1.051 mm using a 100-mm-long cavity; LNP ($LiNdP_4O_{12}$) at 1.048 mm using a 140-mm-long cavity; and Nd:GSGG ($Nd_xGd_{3-x}Sc_2Ga_3O_{12}$) at 1.061 mm using a 625-mm-long cavity. In each case, single-longitudinal-mode, single-spatial-mode operation was achieved with pump powers many times above threshold.

The mechanical stability of such microchip lasers are improved by depositing the dielectric mirrors directly onto the solid-state gain media. The gain crystals were first cut into large diameter wafers, and polished to the desired thickness. Dielectric cavity mirrors were then deposited directly onto the crystals, before they were cut into small pieces. Microchip lasers using two different gain media, Nd:YAG and LNP, were created in this way, and are discussed below.

A $Ti:Al_2O_3$ laser operating near 808 nm was used as a pump source to characterize the microchip lasers. The 1.064-mm Nd:YAG microchip lasers had a lasing threshold below 0.7 mW of absorbed power, and the slope quantum efficiency (determined from the output of the laser from the 99.7% reflecting mirror only) of greater than 46%. The far-field pattern of the output beam was circularly symmetric, and almost perfectly gaussian, as shown in Fig. 1. The divergence of the beam was about 20 mrad, corresponding to a fundamental-mode waist of approximately the same size as the pump spot in the Nd:YAG (about 50 μm).

Spectrometer traces of the output beam of the Nd:YAG microchip lasers showed only single-longitudinal-mode operation for absorbed pump powers up to 40 mW. The lasing frequency tuned

slightly as the pump spot on the microchip cavity was moved to positions with a slightly different cavity length. The devices constructed with wafer mirrors were continuously tunable over the entire gain spectrum by mechanical movement of the mirrors. The maximum single-frequency power obtained from the 730-mm-long Nd:YAG microchip lasers operating at 1.064-mm was 22 mW and the output was polarized to better than 1 part of 300.

The linewidth of the 1.064-mm Nd:YAG microchip lasers has been measured by heterodyning the output of two free-running devices together. The outputs of these microchip lasers were stable enough to obtain heterodyne measurements with a resolution of 10 kHz. At this resolution, the measured spectral response was instrument limited, giving a linewidth for the microchip lasers of less than 5 kHz, assuming equal contributions to the linewidth from each laser. The theoretical phase-fluctuation linewidth is estimated to be only a few hertz. The heterodyne spectrum of the 1.064-mm Nd:YAG microchip laser is shown in Fig. 11. Relaxation oscillations account for the observed sidebands 700 kHz away from the main peak. At higher pump powers these sidebands have been moved to greater than 1 MHz away from the main peak. The intensity of the sidebands varied with time, but was always greater than 30 dB below the main peak. With increased stability of the pump source, as might be obtained with diode pumping, the magnitude of the relaxation sidebands should decrease considerably.

The LNP lasers had a cavity length of 140 mm. The output mirror had a reflectivity of 98.7% at the lasing wavelength, and transmitted the pump. The opposite mirror had a reflectivity of 99.9% at the lasing wavelength and a 75% transmittance for the pump. Measurements showed that 25% of the incident pump power was reflected by the laser package and 10% was transmitted. The threshold for lasing was measured to be about 3.4 mW of absorbed power, and the slope quantum efficiency was 28%. The LNP microchip lasers ran single-frequency for all available pump powers. The maximum single-frequency output obtained was 26 mW, and was pump power limited. The far-field pattern of the output beam was nearly circularly symmetric, indicating a good TEM_{00} mode.

The microchip lasers have been pumped with the unfocused output of GaAlAs diode lasers. The microchip laser is placed in front of the output facet of the diode laser and longi- tudinally pumped without any focusing lens. The distance between the diode and the microchip is adjusted so that the resulting pump spot in the microchip cavity is nearly circular, giving a circular far-field pattern. The divergence of the output beam is diffraction limited, with a fundamental-mode waist that is approximately the same size as the pump spot. The almost perfectly gaussian far- field profiles are shown in Fig. 3.

The performance of diode-pumped microchip lasers is similar to the performance of $Ti:Al_2O_3$-pumped devices. As an example, the 1.32-mm Nd:YAG microchip laser discussed above was pumped with a 480-mW diode laser. The output showed single-frequency, TEM_{00} operation at all available diode pump powers. The maximum cw output power obtained was 51 mW. The output beam had a divergence of 8 mrad, corresponding to a 200-mm pump spot in the microchip cavity. The slope quantum efficiency of the microchip laser was greater than 40%, and the overall wall-socket efficiency (electrical input to 1.32-mm optical output) was greater than 4%.

Because of the extremely short cavity length of the microchip lasers, a small change in cavity length results in a large change in output frequency of the device. A 1.06-mm Nd:YAG microchip laser, for example, with a 650-mm-long cavity tunes at a rate of 460 MHz per nm of cavity length change. By applying a transverse stress to small, monolithic, Nd:YAG lasers their length can be changed enough to tune them over a large portion of the gain bandwidth of the Nd:YAG. With the proper choice of cavity length, the microchip lasers can be designed to have a single-frequency tuning range as large as the gain bandwidth of the gain medium, constrained by the pump power requirements of the laser and the absorption length of the gain crystal. These lasers operated in a single longitudinal and transverse mode. In the absence of an applied stress their polarization was randomly oriented. Once stress was applied, the polarization of the microchip lasers was parallel to the direction of the stress, consistent with earlier experiments which have been reported in the literature. To dynamically tune the 1.064-mm, single-frequency, Nd:YAG microchip lasers, crystals were tightly fitted into U-shaped holders adjacent to a PZT piezoelectric transducer, as shown in Fig. 12. A voltage was applied to the transducer of the tunable laser, which in turn applied stress to the Nd:YAG in a direction orthogonal to the laser cavity, changing the cavity length. Single-frequency, single-polarization operation was observed over the entire stress-tuning range. Figure 13(a) shows the heterodyne spectrum of a frequency modulated microchip laser with a sine wave drive applied to the PZT compared to the theoretically expected spectrum in (b). The deviation of the spectrum from the expected theoretical curve is due to the frequency response of the heterodyne system, which is not flat over the entire range.

The small cavity lengths of microchip lasers lead to very short cavity lifetimes, even for cavities with high reflectivity mirrors. As a result, microchip lasers are capable of producing pulses that are shorter than can be obtained with larger solid-state lasers. To obtain pulsed operation of the microchip lasers, they were pumped with a pulsed $Ti:Al_2O_3$ laser. The output of the $Ti:Al_2O_3$ laser was a train of 40-ns pulses (full width at half maximum) at a 5-kHz repetition rate, with a time averaged power of 180 mW. When the $Ti:Al_2O_3$ laser was tightly focused onto the microchip lasers strong relaxation spiking was observed. The pump was defocussed until each pump pulse produced one output pulse. At that point the temporal and spectral profile of the microchip pulse was measured.

Gain-switched pulses have been obtained from several microchip lasers. One was constructed from Nd:YAG, with a 730-mm-long cavity and a 1.3% output coupler at 1.064 mm. The output pulse from such a laser had a duration of 760 ps. This pulse width is comparable to the calculated microchip cavity lifetime of 650 ps. The peak pulse power was about 5 kW. Spectral measurements showed that only one longitudinal mode of the microchip laser was oscillating. Visual inspection of the far-field pattern indicated that the laser was operating in the TEM_{00} mode.

A second pulsed microchip laser consisted of a 140-mm-long LNP cavity with a 1% output coupler at 1.048 mm. It was difficult to adjust the $Ti:Al_2O_3$ pump laser so that each of the pump pulses consistently resulted in only one output pulse from this device. A streak camera was used to measure an output pulse width of only 80 picoseconds. As in the case of the pulsed Nd:YAG microchip laser, the pulsed LNP microchip laser operated at a single frequency in the TEM_{00} mode. Unlike modelocked pulses, gain-switched pulses can be individually generated. The experiments described above demonstrate that it is possible to obtain very short, single-frequency, gain-switched pulses from microchip lasers. The duration of the output pulse is limited by the microchip cavity lifetime. By decreasing the cavity lifetime, through the use of lower reflectivity output mirrors or shorter cavities, it should be possible to produce microchip lasers with single output pulses of much less than 80 ps.

The low pump threshold, high efficiency, and single-frequency operation of microchip lasers makes diode-pumped microchip lasers extremely promising. The tuning capabilities of microchip lasers are unique. Larger lasers may be tuned in the same manner as microchip lasers, but the longer cavity length greatly restricts both the tuning range and rate. Only the microchip laser allows the possibility of continuous, single-frequency tuning across the gain bandwidth of the laser at an arbitrary rate, up to the limit imposed by the cavity response time. The short cavity length of the microchip lasers, and the resulting short cavity lifetime, also permits the generation of very short gain-switched pulses.

The simple fabrication of microchip lasers, and the ability to pump them with commercially available diode lasers, should help to make them attractive for a large range of applications.

The use of semiconductor diode laser arrays as pump sources will allow for much higher power operation of solid state lasers. One of the advantages of solid state lasers over semiconductor lasers is the energy storage capability of such materials and the subsequent extraction of this energy in a short time resulting in very high peak power output. Figure 14 shows a Nd:YAG laser which is pumped by GaAlAs diode laser arrays. These arrays are made up of one cm bars of lasers eight of which are bonded onto a silicon heat sink into which has been etched 45 degree angled mirrors to deflect the output radiation in a direction orthogonal to the surface of the array. Other diode laser array geometries include the well-known rack and stack in which laser array bars are bonded onto individual copper heat sinks and then stacked together to form a two-dimensional array. With presently available commercial diode laser array technology, it would be possible to make a 100 watt cw or average power, diffraction limited Nd laser at 1.06 μm which could in turn be frequency doubled into the visible with possible power levels of tens of watts. Such a laser could become a replacement for the commercial high power ion laser.

APPLICATIONS

Lasers have already been used in a wide variety of applications for many years. The most well known of these are fiber optical communications, compact disc and laser printers. One of the major advantages of the solid state and semiconductor laser devices described here in their ability to operate efficiently and reliable and to be scaled either up or down in power. One often neglects the importance of being able to operate a laser efficiently or at all at low power levels. Some of the most important applications of solid state and semiconductor laser technology that will come about in the next ten years are listed below.

PROJECTION DISPLAY

The availability of small diode pumped solid state lasers which can be frequency doubled into the red, blue and green spectral regions will allow their use in high resolution projection display for movie theater and home television. The advantages of laser projection display are high resolution, high brightness with far less edge falloff, constant focus independent of the screen surface and adjustable screen area. The laser projection system will mean that either front or back projection is possible and will eliminate the vacuum tube for larger area screen television. Figure 15 shows a schematic for a how such a laser projection system might look. This market could emerge as one of the largest for lasers in the next decade and amount to tens of billions of dollars in systems sales.

LASER PRINTERS

Laser printers are now in wide use throughout the world. With the advent of lower cost devices which operate in a circularly symmetric diffraction limited output of about one watt cw, high speed and low cost color printers will be made available for the home market for use in FAX machines and for color printing associated with electronic photography.

OPTICAL DISC TECHNOLOGY

Low cost diffraction limited visible or UV lasers will allow for high density read and write disc applications such as computer memory and video recording. Cameras will be able to store high resolution images in such discs with such high density that motion picture cameras will be sold rather than still frame cameras.

WAVELENGTH MULTIPLEXED OPTICAL COMMUNICATIONS

Fiber optical communications presently uses diode lasers operating at 1.3 and 1.5 μm and achieve data rates of more than one Gbit. Future information needs will require higher data rates. Increasing the speed for a single diode laser causes difficulties in the ability to electronically process the bit stream. The use of a laser which can be frequency tuned will allow for wavelength division multiplexing. Such lasers, however, must be low cost and reliable. Wavelength calibration techniques must be developed in order that a standard frequency system be used for compatibility when different lines are connected together. Wavelength multiplexed systems would find important use in computer communications systems.

ROBOTICS AND MACHINE CONTROL

Laser radar techniques have been well developed over the last twenty years and could become a practical tool as the eyes of robotic systems. For widespread use, however, the cost and reliability must be improved. The recent developments in solid state lasers has now made this closer to reality. Low cost, single-frequency microchip lasers could be used as transmitters as well as local oscillators for short range imaging radar systems for robotic control. Similar lasers could be used for precision motion control devices for application to machine tool control systems and for precision orthogonal control for the semiconductor industry. In particular, low cost three- dimensional control systems would revolutionize the manufacturing industry.

LASER MEDICINE AND MEDICAL DIAGNOSTICS

Lasers are presently being used for numerous applications in the medical area. Some of these areas are listed here together with some of the types of new solid state and diode lasers that will be important for these applications.

Lithotripsy (stone destruction)

Multiwavelength solid state lasers. 589 nm, for example, at 10's of mJ in μs to ns pulses.

Ocular Surgery - Retinal Photocoagulation

Diode lasers, 1-3 watts cw with millisecond pulses.

Angioplasty

Tunable solid state lasers such as Ti:sapphire with frequency shifting

Cancer Treatment

Tunable solid state or diode lasers at 1-10 watt average power.

Dermatology

Tunable solid state lasers or diode lasers. 1-100 mJ or a few watts CW.

The present laser market for 1989 is about $700 million. The above fields of use are expected to increase the laser applications market into the tens of billions of dollars per year during the next decade.

$Ti:Al_2O_3$ SINGLE CRYSTAL

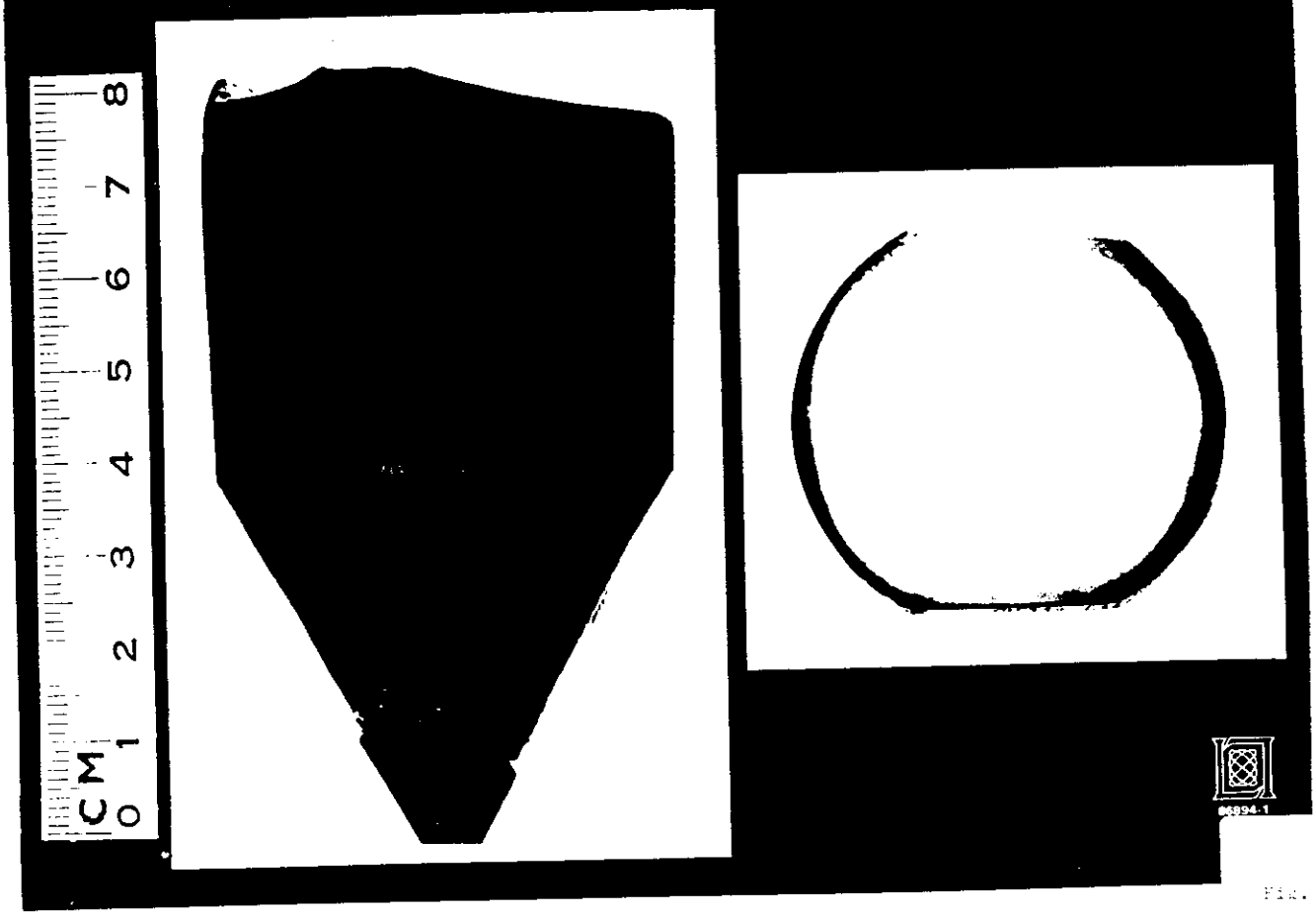

TUNING CHARACTERISTICS OF $Ti:Al_2O_3$ LASER

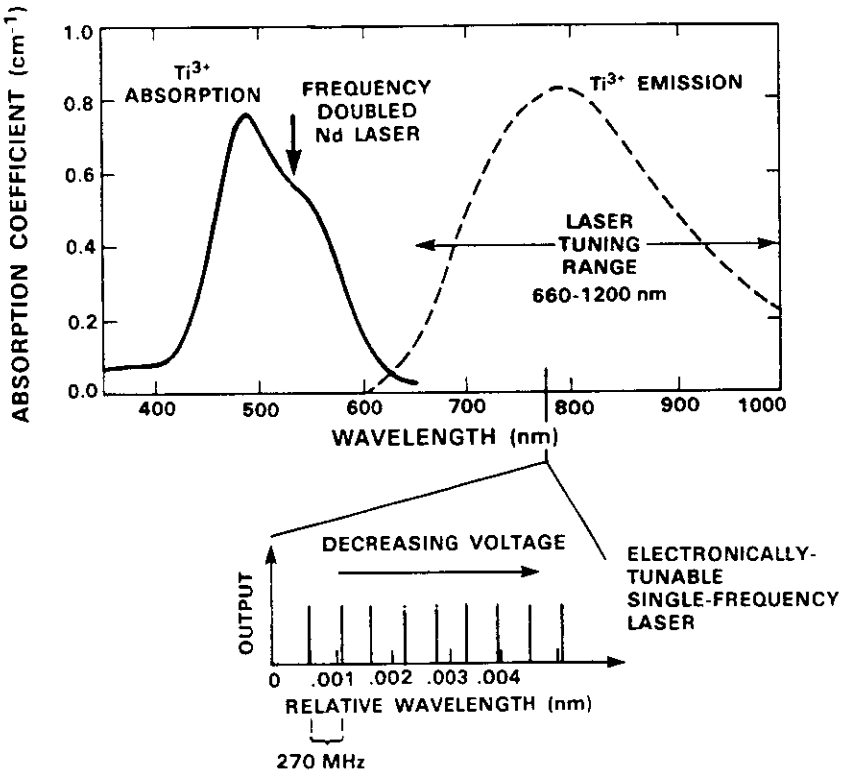

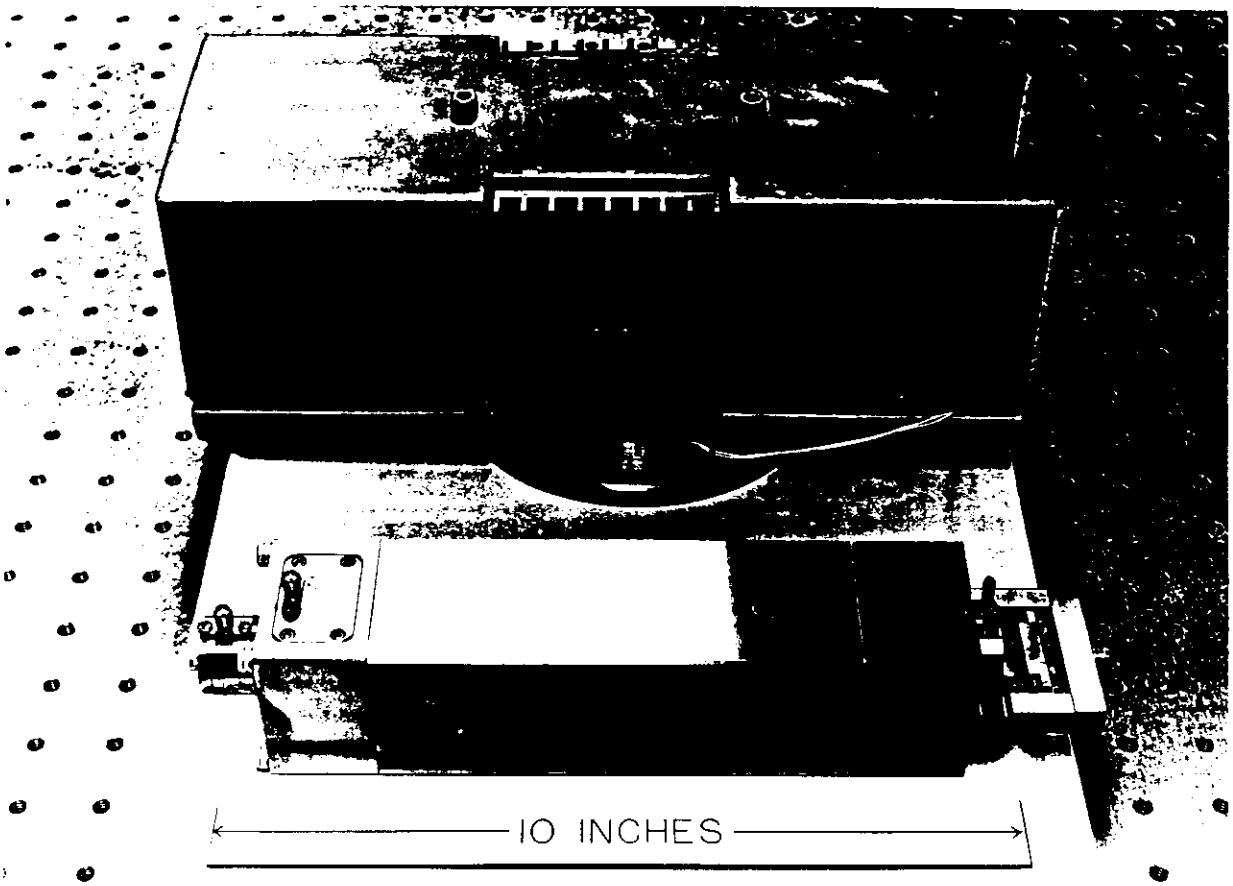

Fig. 3

SPECTRAL OUTPUT OF MONOLITHIC AND EXTERNAL CAVITY GaAlAs DIODE LASER

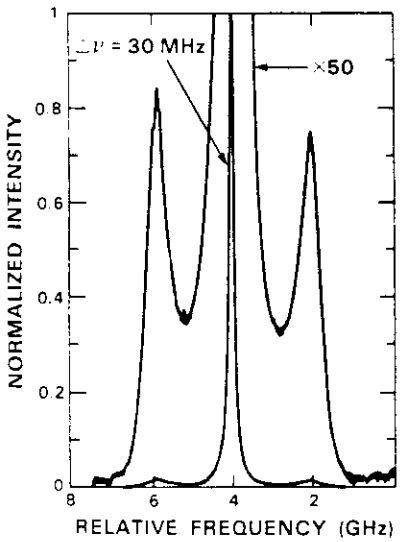

FABRY-PEROT
SCAN OF MONOLITHIC
DIODE LASER

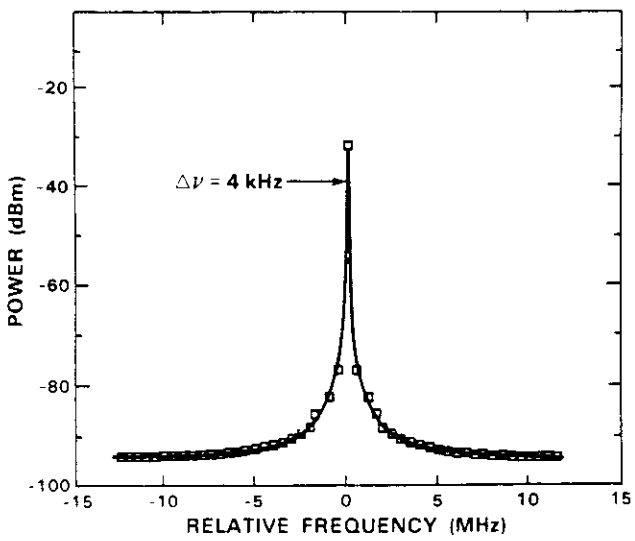

HETERODYNE BEAT
BETWEEN TWO EXTERNAL
CAVITY DIODE LASERS

80003-5

Fig. 4

HETERODYNE BEAT SIGNAL BETWEEN TWO FREE RUNNING EXTERNAL CAVITY (GaAl)As DIODE LASERS

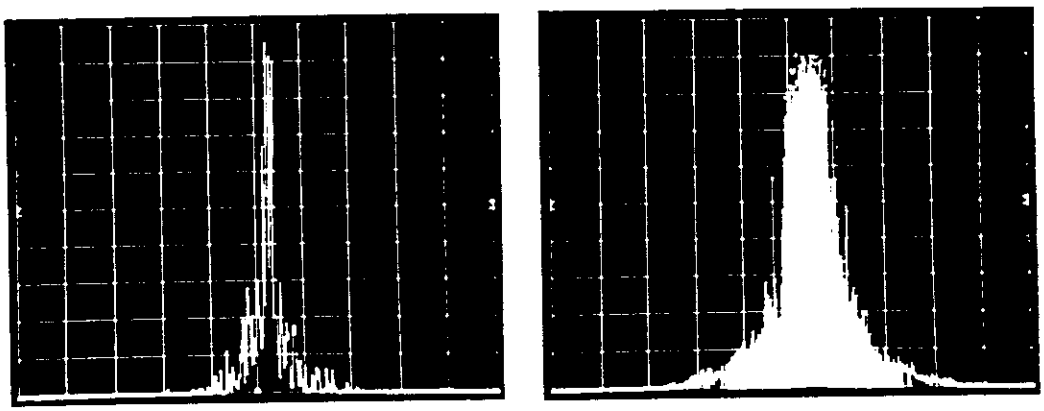

30 ms SCAN

60 s SCAN

100 kHz/div, 10 kHz RESOLUTION BW

79143-2

Fig. 5

HETERODYNE SPECTRUM OF PHASE-LOCKED EXTERNAL CAVITY (GaAl)As DIODE LASERS

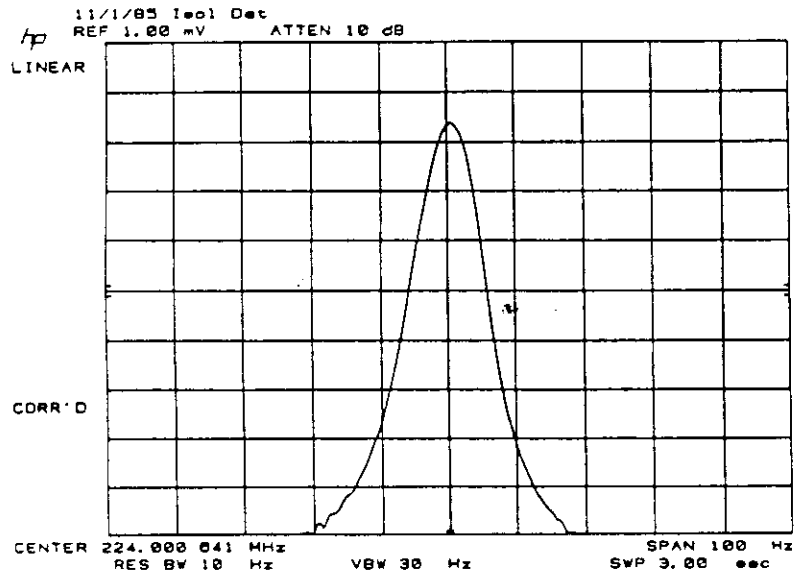

10 Hz/DIV, 10 Hz RESOLUTION BW
224.000641 MHz Center Frequency

OUTPUT POWER vs CURRENT UNCOATED GRIN-SCH-SQW LASER

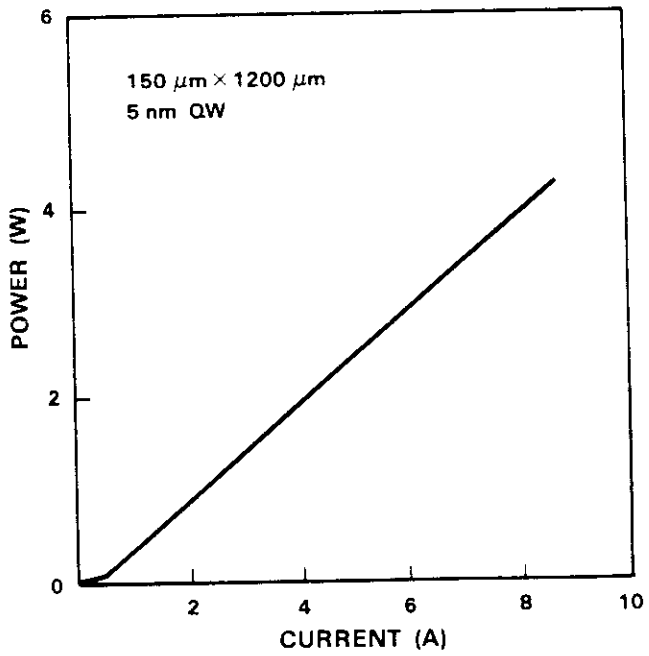

107110-1

Fig. 7

SINGLE-FREQUENCY MICROCHIP LASER

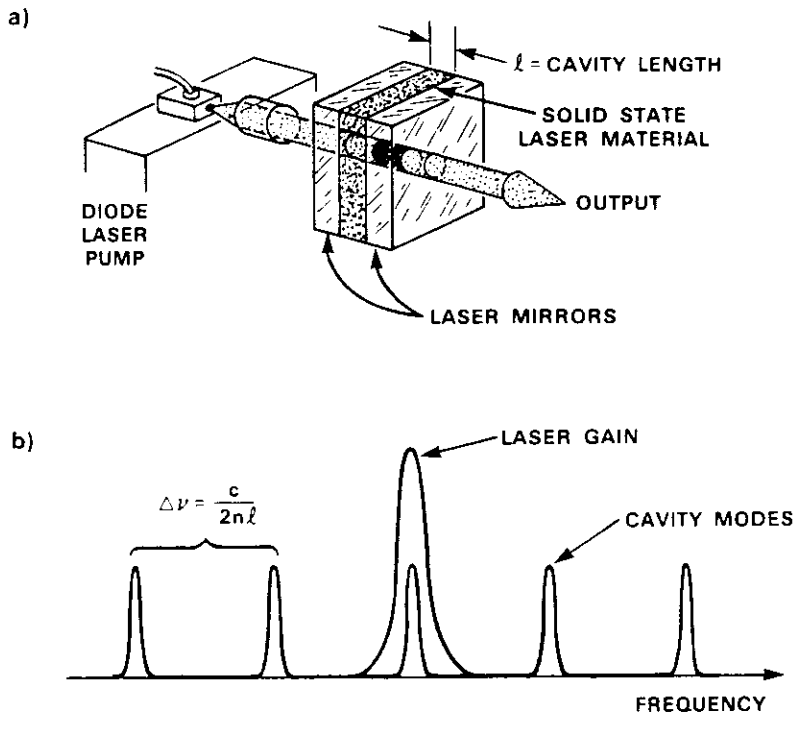

103649-1

Fig. 8

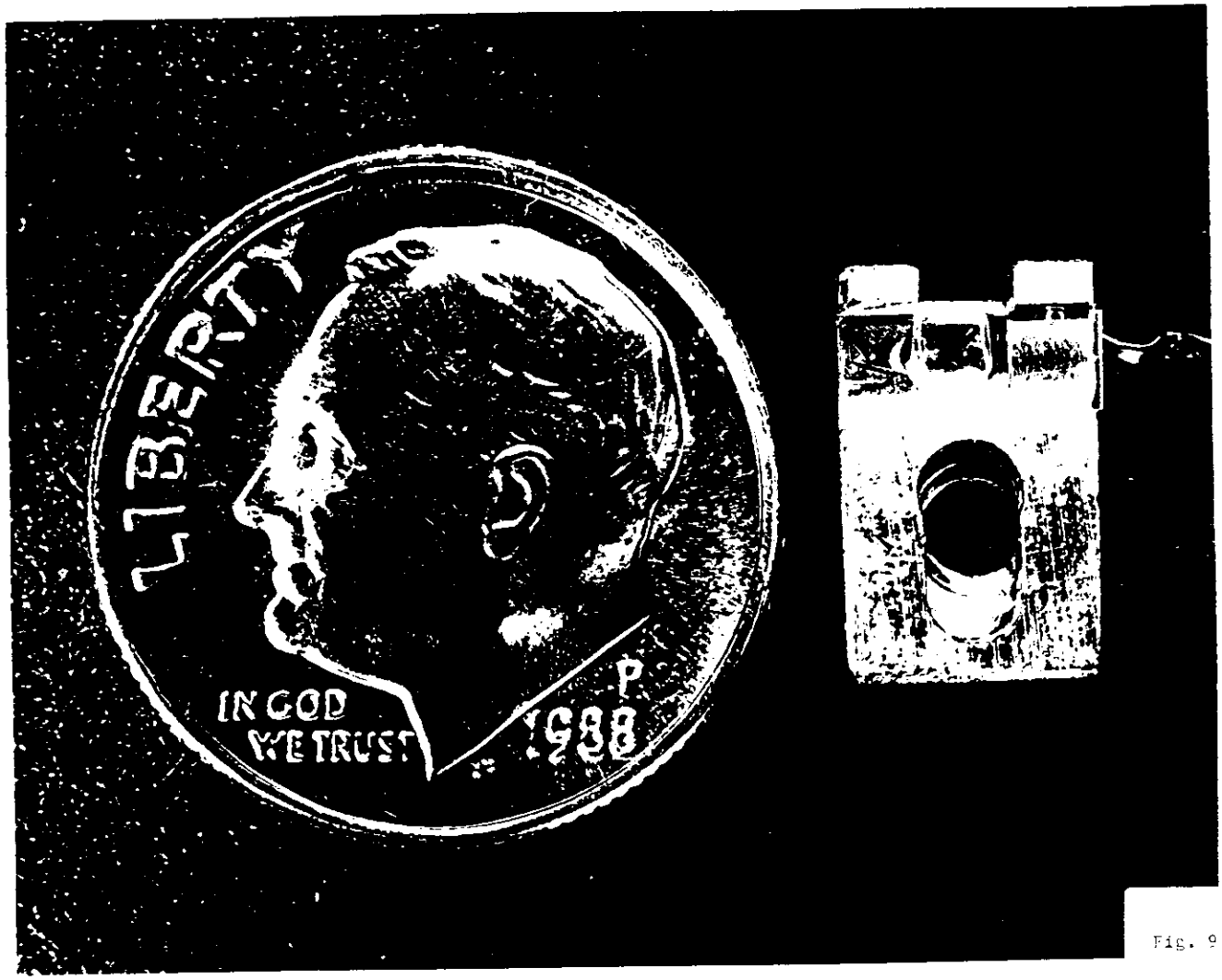

Fig. 9

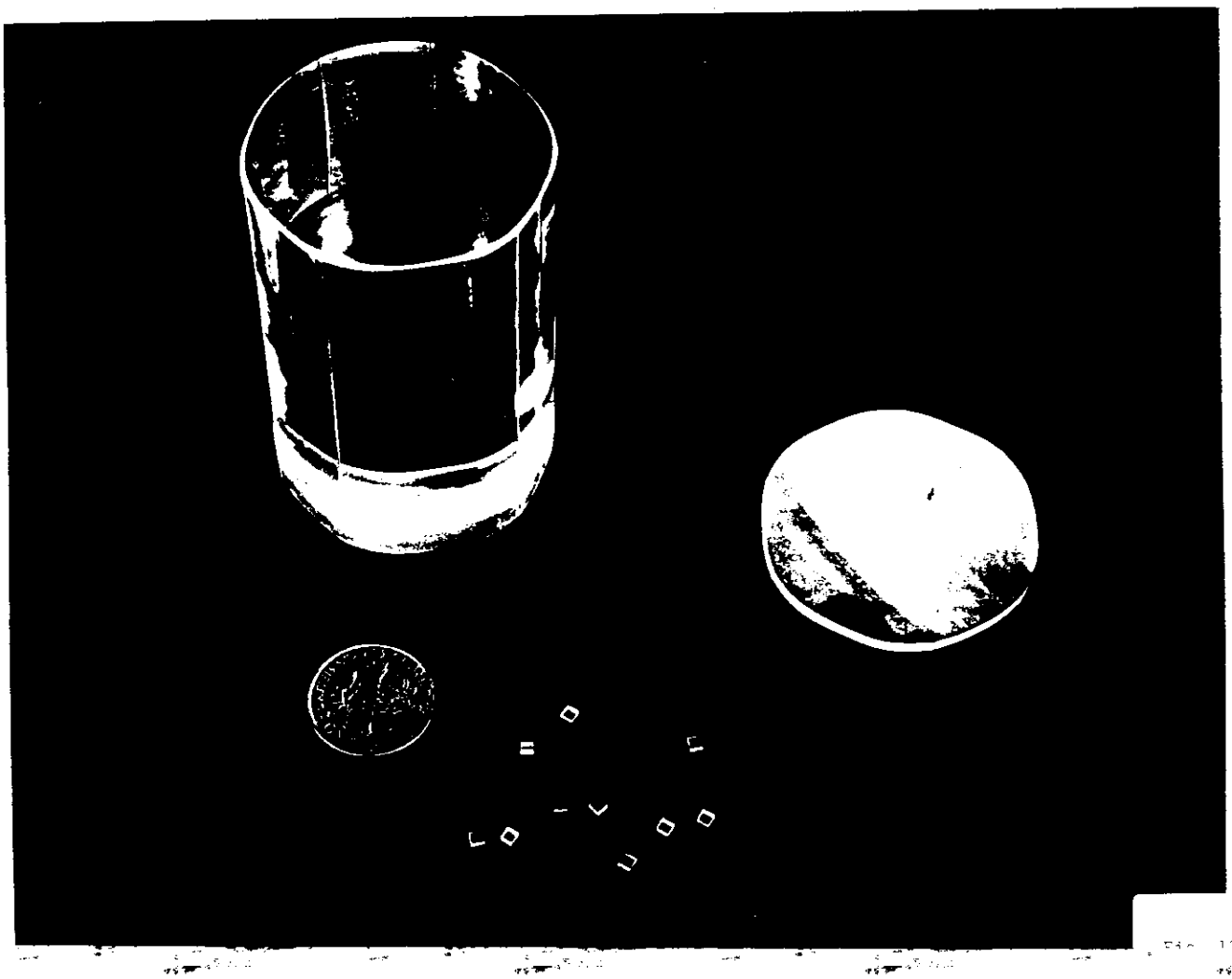

Fig. 10

HETERODYNED Nd:YAG MICROCHIP LASER SPECTRUM

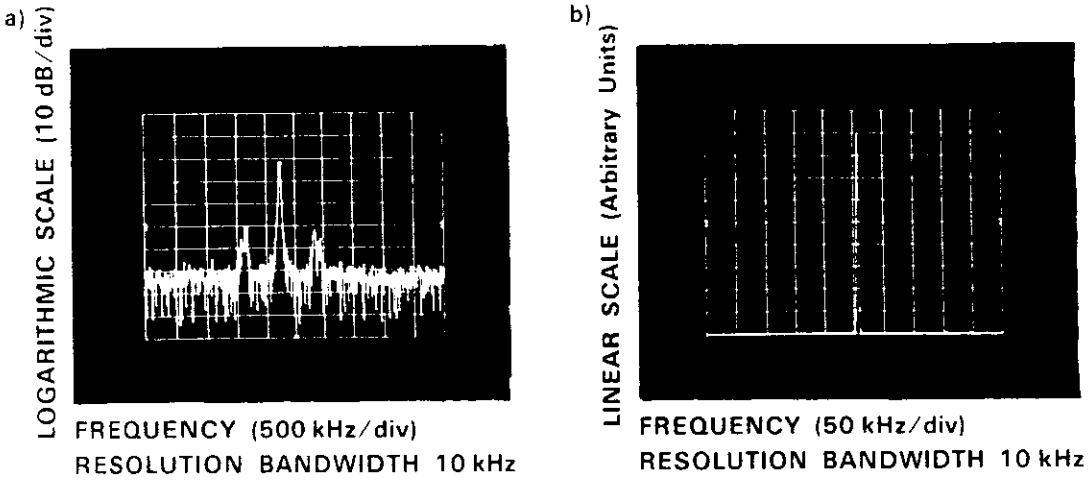

103649-2

Fig. 11

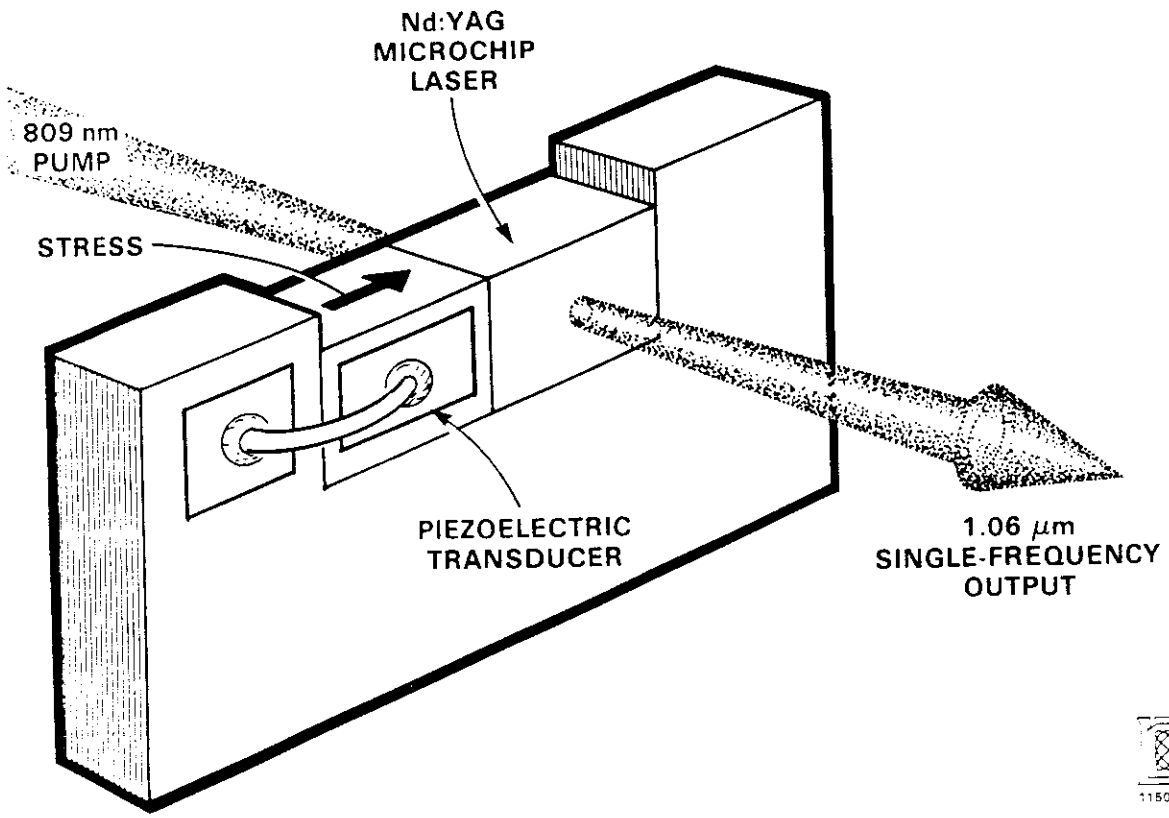

115003-1

Fig. 12

PIEZOELECTRIC TUNING OF SINGLE-FREQUENCY Nd:YAG MICROCHIP LASERS

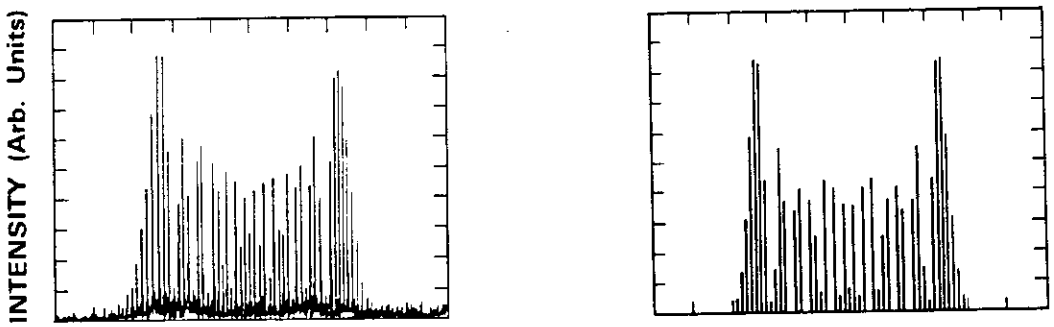

Fig. 13

10-W DIODE ARRAY PUMPED Nd LASER MODULE

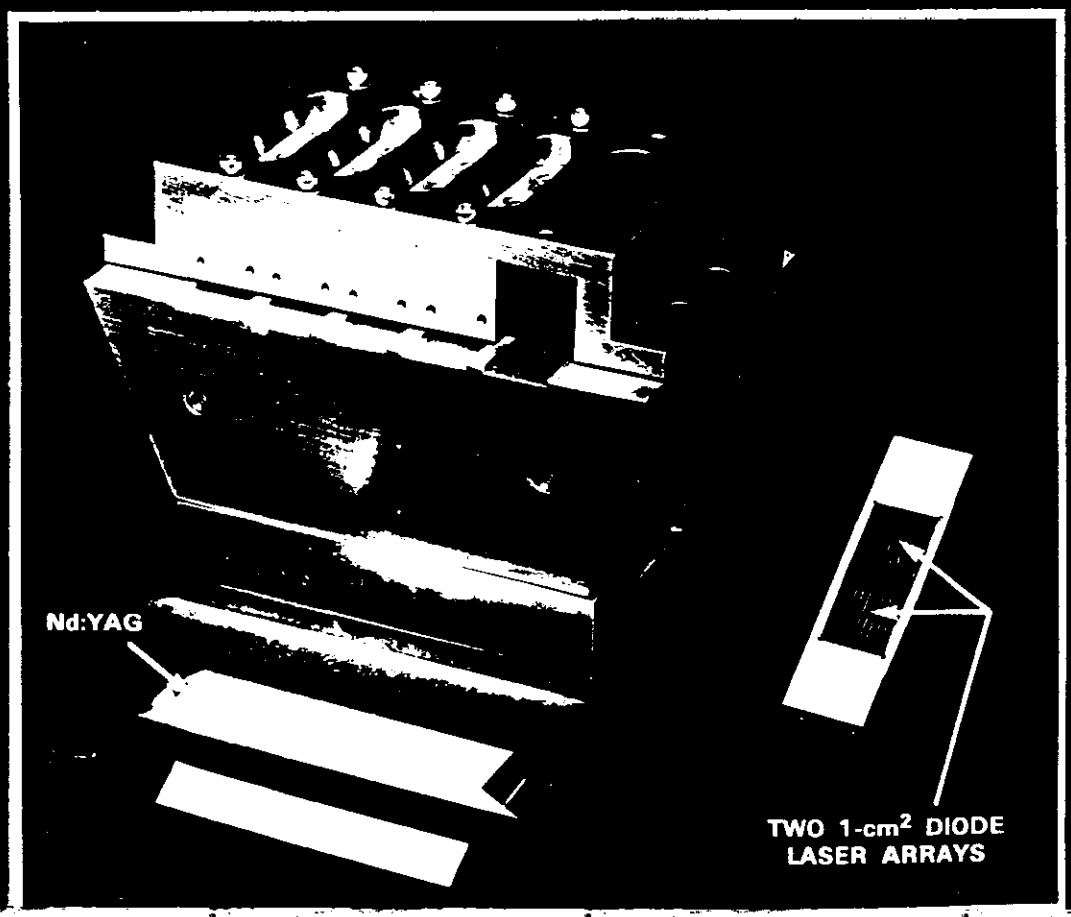

Fig. 14

LASER HDTV

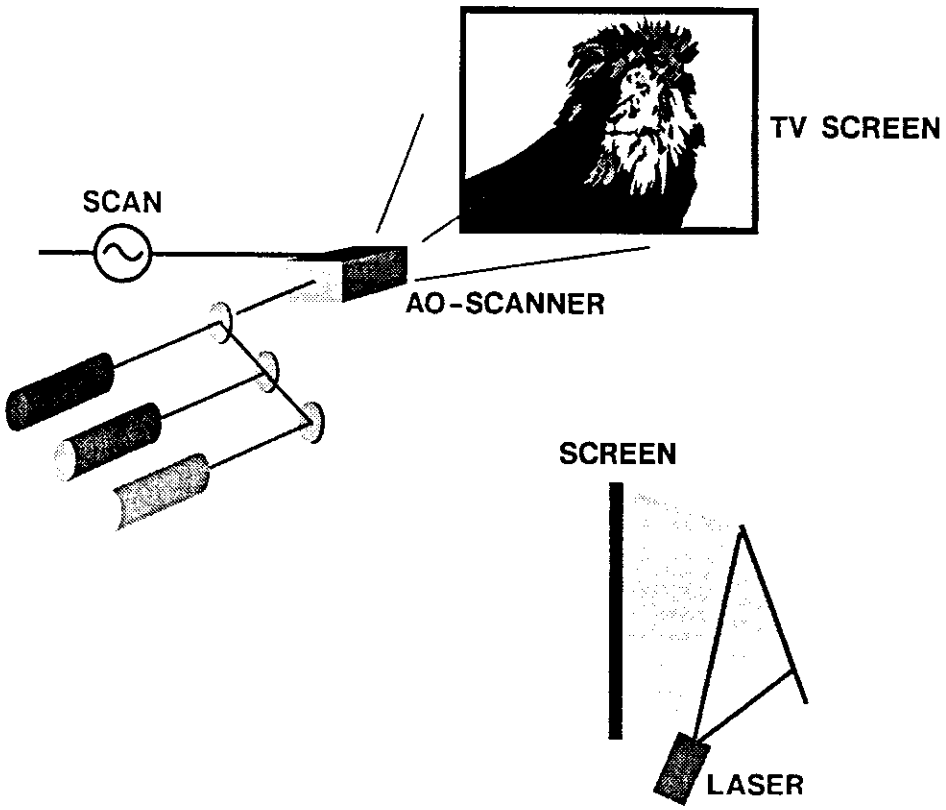

Fig. 15

133832-1